SELECTION OF MATERIALS AND MATERIAL RELATED PROCESSES FOR FCC POWER RECOVERY TURBINES

by
Phillip Dowson
General Manager Materials Engineering
and
David Dowson
Service Engineer (Repairs)
Elliott Company
Jeannette, Pennsylvania

Phillip Dowson is General Manager, Materials Engineering, with Elliott Company, in Jeannette, Pennsylvania. He has 37 years of experience in the turbomachinery industry. Mr. Dowson is responsible for the metallurgical and welding engineering for the various Elliott product lines within the company. He is the author/coauthor of a number of technical articles, related to topics such as abradable seals, high temperature corrosion, fracture mechanics, and welding/brazing of impellers, and has been awarded numerous patents.

Mr. Dowson graduated from Newcastle Polytechnic in Metallurgy and did his postgraduate work (M.S. degree) in Welding Engineering. He is a member of ASM, NACE, ASTM, and TWI.

David Dowson is a Service Engineer (Repairs), with Elliott Company, in Jeannette, Pennsylvania. He has been involved with material related failure analysis, repairs to rotating and nonrotating equipment, and aftermarket support.

Mr. Dowson received his B.S. degree (2003) from the University of Pittsburgh.

ABSTRACT

Fluid catalytic cracking (FCC) power recovery turbines have been in existence for over 50 years and through the years many changes have been made to design, materials, and material related processes. This paper highlights how materials are specified for the various components and what material properties/factors one has to consider for the application. Both rotating and nonrotating components will be reviewed for material selection.

Due to the aggressive corrosion and erosion environments, selection of various coatings must be made that are resistant to aggressive environment. A number of various coatings for both erosion and high temperature corrosion resistance will be discussed.

Components such as turbine disks, blades inlet/exhaust casings are costly to replace and delivery can be long. Consequently, their components need to have design proven repair procedures to minimize replacement costs and long lead times. This paper will highlight the various repair procedures and the technical support required for supplying a functional quality component.

This paper will outline the remaining life assessment procedures and review the various damage mechanisms such as creep, fatigue, creep fatigue and various embrittlement mechanisms that can occur in FCC power recovery turbines. Also highlighted will be the various testing methods for determining life or life extension of components such as high precision stress relaxation (STR) test, which determines creep strength, and constant displacement rate (CDR), which evaluates fracture resistance. Other tests such as replication/microstructure analysis will also be reviewed for calculating the remaining life or life extension of the components.

INTRODUCTION

In the typical refinery, fluid catalytic cracking (FCC) processes low value feedstocks are converted to various petroleum products, such as gasoline in a reactor vessel with the aid of hot catalyst. In this process, feedstocks are cracked into low boiling fractions, such as light olefins and high octane gasoline. After cracking, the spent catalyst is covered with coke deposits that must be removed prior to its reuse. In addition to carbon, heavy metals and sulfur are deposited on the catalyst surface. Recycling takes place in a regenerator where the coke is burned off by blowing hot air. The combustion products or flue gases that result from this recycling are a source of recoverable energy. The major components of the FCC process are illustrated in Figure 1.

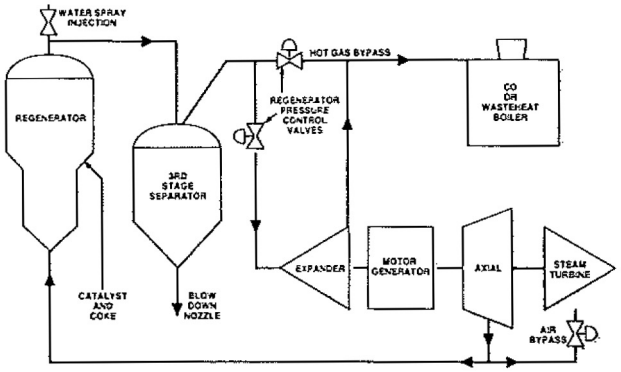

Figure 1. Major Components Associated with the FCC Power Recovery Process.

As energy costs increase, the importance of efficiency in each process increases. This is certainly true for the fluid catalytic cracking process where energy is recovered from the hot pressure discharge flue gas in a hot gas expander. Depending on customer requirements, expanders can deliver between 3,000 to 60,000 shaft horsepower. Typical flue gas inlet temperatures can vary from 1200 to 1400°F (649 to 760°C) at a pressure of 16 to 35 psig whereas exhaust temperatures may range from 950 to 1100°F (510 to 593°C) at pressures of 1.0 to 3.0 psig. The mass flow rates through the power recovery turbines can vary from 110,000 to 1,700,000

lbm/hr. Typically today FCC power recovery turbines are single stage units. The single stage unit is schematically illustrated in Figure 2.

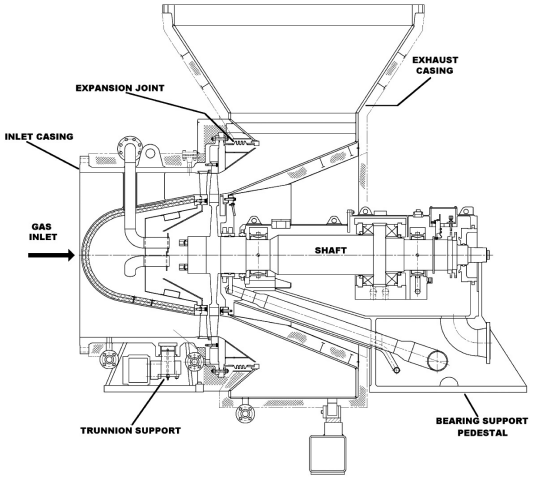

Figure 2. Cross Sectional View of a Single Stage FCC Power Recovery Turbine.

In today's marketplace, selection of materials for various components for hot gas expanders is very competitive and an important factor in the overall cost and delivery of the product. Due to the high temperature that the material will be subjected to, material selection becomes an important factor in the design of the unit. Various temperature dependent processes such as corrosion rate and degradation mechanism such as creep must now be considered. Also, FCC expanders operate in environments that can be very erosive. The source of the erosion is spent catalyst from the FCC process that has not been recovered by separators and cyclones. For protection against aggressive corrosion or erosion mechanism, various coatings have been successfully applied.

The choice of materials for rotating and stationary components of hot gas expanders requires a selection based upon a number of design and environmental factors. The design factors that require consideration are the properties of the material together with the operating requirements of the units (such as gas composition/temperature/catalyst particle in gas steam, etc.).

For hot gas expander materials, this paper will highlight the following areas:

- Material selection of rotating equipment such as disk, blades, bolting, etc.
- Material selection of nonrotating equipment such as inlet and exhaust casing, expansion joint casing supports, bolting, etc.
- Aggressive corrosion and erosion environments
- Repairs of costly to replace/delivery of components such as turbine disks, blades, inlet/exhaust casing, stator blades
- Remaining life assessment of hot gas expander components

MATERIAL SELECTION OF ROTATING EQUIPMENT SUCH AS DISKS, BLADES, BOLTING, ETC.

Material selection considerations include good elevated temperature mechanical properties that include not only the normal parameters like yield strength, ductility, and endurance strength, but special temperature-related properties such as:

- Creep.
- Stress rupture.
- Low cycle fatigue.
- Thermal conductivity.
- Thermal expansion.
- Hot corrosion resistance.
- High temperature hardness.

Disks

Over the years, hot gas expander disks have utilized materials such as A286, Inconel® 718, and the most common Waspaloy® (AISI 685). The selection of the material for the disk depends upon the inlet temperature and the applied stress at the root of the blade insert. When the gas conditions are in a partial combustion state, consideration must be given for protection against high temperature corrosion that can lead to premature failure (Figure 3). This premature failure is an embrittlement of the material that can occur with most, if not all, nickel base alloys under certain temperature/stress and environment conditions. This embrittlement phenomenon will be discussed later in the paper. Due to the high temperature corrosion phenomenon, the authors' company developed a new alloy called RK1000, which is four times the protection against high temperature corrosion as compared to Waspaloy.

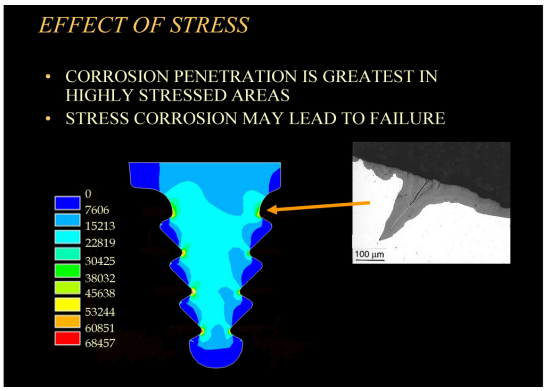

Figure 3. Showing Location of Highest Stress at Root of Blade.

In the high temperature regions, creep and creep rupture are a concern. The traditional approach is to use a Larsen-Miller plot as shown in Figure 4. The design stresses are generally based on 10^5 hours smooth bar creep rupture stress values divided by some appropriate safety factor.

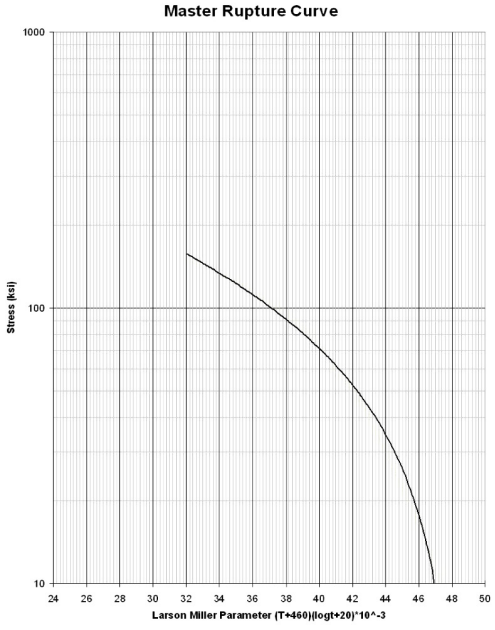

Figure 4. Larsen-Miller Rupture Curve for Waspaloy.

In the early 1950s vacuum induction melting was introduced by the Kelsey Hayes Company (later Special Metals Company), which dramatically improved the quality and properties of existing nickel-base alloys. The vacuum melting process removes oxygen and nitrogen from the melt and, thereby, prevents their reaction with aluminum (Al) and titanium (Ti) to form oxide and nitride inclusions. Consequently, the elements Al and Ti are thus retained for subsequent precipitation. The vacuum refinery also removes volatile impurities such as bismuth and lead. Consequently, the net results are an improvement in stress rupture properties as well as forge ability (work ability). Work done by Darmara (1967) reported a three to four improvement in stress rupture life of Waspaloy by vacuum melting compared to heats made by best arc melting procedure. Today Waspaloy disks are manufactured from vacuum induction melted ingots followed by vacuum arc remelting. Both Inconel® 718 and A286 allow electroslag remelting for smaller disks providing the ingots have been vacuum induction melted. A great deal of work has been done by the authors' company in evaluating air melted A286 mechanical properties. Substantial testing has indicated that air melted A286 material even with electroslag remelting has inferior creep/creep rupture properties compared to vacuum melting material. Testing performed has indicated that in the 1000°F to 1100°F (538°C to 593°C) temperature range, A286 can be notch sensitive especially for air melted material. Work done by a special American Society for Testing and Materials (ASTM) task force reviewing failures of disks from A286 material has shown that preferred heat treatments (triple precipitation treatment) can improve the notch sensitivity. The photo in Figure 5 shows an A286 expander disk failure due to notch embrittlement. Table 1 and Figures 6, 7, and 8 show test results of various heat treatments and their corresponding ductilities, which are related to the notch sensitivity of the material (ASTM, 1981/1982).

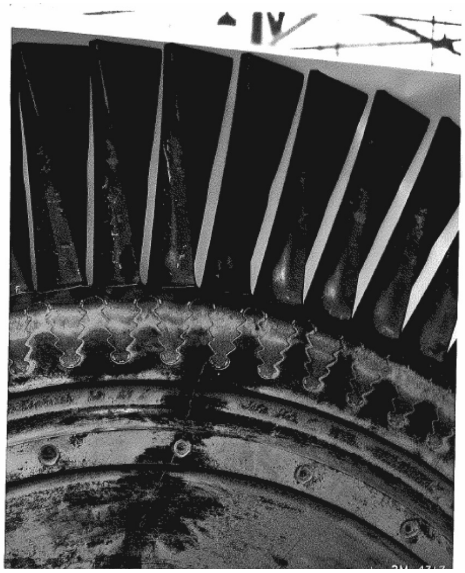

Figure 5. Failed A286 Disk.

Table 1. All Test Pieces Solution Treated at 1800°F (982°C) for One Hour, Oil Quenched. All Aging Treatments Were for 16 Hours and Air Cooled.

Room Temperature Tensile Properties						
No.	**Heat Treatment**	**Tensile Strength, KSI**	**Yield Strength, KSI**	**Elong., %**	**RA, %**	**Hardness R_C**
1	1800°F (982°C) + 1325°F (718°C)	151.1 150.3	98.7 101.1	26.0 26.0	26.7 40.5	30
2	1800°F (982°C) + 1325°F (718°C) + 1200°F (649°C)	160.8 156.0	110.6 109.6	26.0 25.0	38.4 38.8	32
3	1800°F (982°C) + 1375°F (746°C) + 1200°F (649°C)	160.0 158.8	115.2 113.6	22.0 22.0	35.4 37.3	33
4	1800°F (982°C) + 1425°F (774°C) + 1200°F (649°C)	149.8 152.7	99.1 103.9	25.0 21.0	38.5 37.5	33

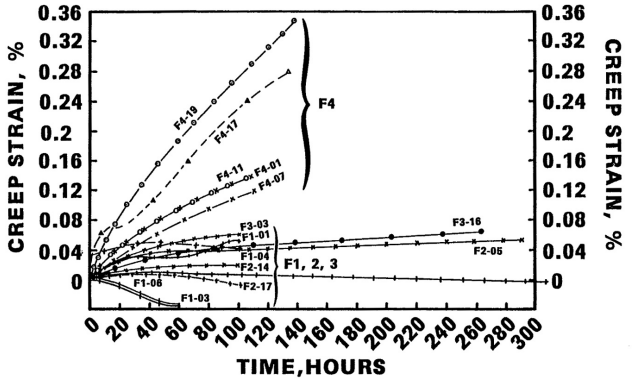

Figure 6. A286 Creep Curves Displayed by Material in Four Different Heat-Treated Conditions on Loading to 85,000 PSI at 1000°F (538°C).

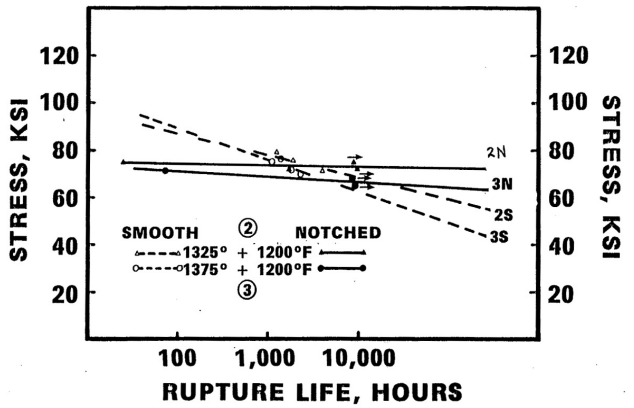

Figure 7. Stress-Rupture Curves on Smooth and Notched Specimens at 1100°F (593°C) for Material in Conditions 2 and 3.

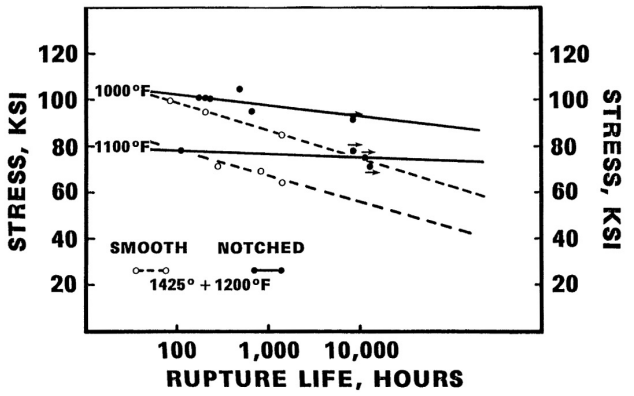

Figure 8. Stress-Rupture Curves on Smooth and Notched Specimens at 1000°F (538°C) and 1100°F (593°C) for Material in Condition 4.

Other recommendations from the task group were to incorporate a creep test to evaluate the notch sensitivity of A286. The authors' company has included this requirement for larger A286 disk materials. When supplying disks made from high temperature materials, such as a superalloy, it is important to detail not only the melting and remelting practices but also the method of forging the disk. Generally, most original equipment manufacturers (OEMs) have a forging process that details the temperature for cogging/upset of the ingot. The authors' company has such a process for each of the materials detailing each step in the forging operation. Nearly all of these disk type forgings are manufactured utilizing close dies. In general there will be a die for each size or inserts to cover various sizes. Figure 9 shows sequence of forging steps.

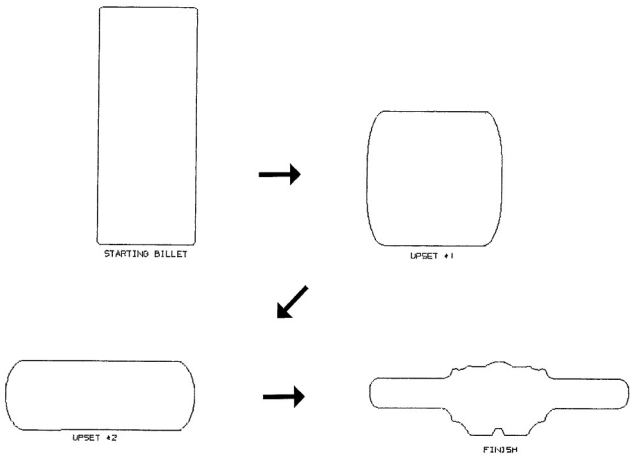

Figure 9. Sequence of Forging Steps.

Machining of these superalloys can be very challenging and some precautionary measures need to be addressed. Generally for A286 most of the machining is performed in the solution treated condition and the final broaching is done in the precipitated heat treated condition. Other processes utilized in shaping the blade slots have been rough cut using electrical discharge machining (EDM) within 0.010 inch followed by broaching for the final dimensions.

For Waspaloy material, especially for large disk type forgings over 24 inches, an additional precipitation hardening treatment is required to improve the notch ductility of the material. The additional precipitation hardening treatment is to minimize continuous films of $M_{23}C_6$ carbides within the γ' gamma prime surrounding film (Figure 10). This precipitation treatment forms discrete carbides and reduces the amount of carbon in solution to form these continuous films during operating service. Consequently, the melting, forging, and heat treatment of these superalloys are important in obtaining the required creep/creep rupture strength with good notch ductility. In the past decade, the authors' company invested a great deal of money in developing a new alloy that improved the high temperature corrosion resistance by fourfold. This alloy minimizes high temperature corrosion attack along the grain boundaries (Yakuwa, et al., 1998). The authors' company has applied this material in numerous applications where the process gas is in a partial combustion state. (Partial pressure of oxygen is low and the partial pressure of sulfur is high).

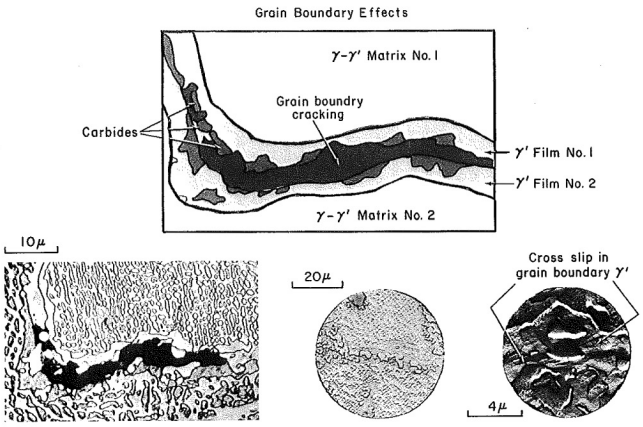

Figure 10. Flow and Fracture Behavior in the Grain Boundary of Waspaloy. (Courtesy Simms and Hagel, 1972)

Table 2 shows the mechanical properties of various materials used for hot gas expander disks and their temperature range application.

Table 2. Mechanical Properties.

	Waspaloy		Inconel 901		A286 (AISI Type 660)	
	Room Temp	1000°F (538°C)	Room Temp	1000°F (538°C)	Room Temp	1000°F (538°C)
Tensile Temperature Min. ksi	175	155	170	135	130	130
Yield Strength 0.2% ksi min	120	105	120	97	85	95
Elongation %	15	15	12	16	15	14
Reduction Area %	18	18	15	22	20	22
Temperature Range °F	1200 to 1400		1100 to 1300		1000 to 1200	
Temperature Range °C	649 to 760		593 to 740		538 to 649	

Rotating Blades

Generally, the materials for blades are very similar to that used for disks. However, other materials such as IN738 cast material, have been used for blades. This material has higher creep strength and can be used at the higher temperatures. Compared to Waspaloy, the material has a lower ductility and, therefore, can be prone to notch ductility issues at the lower operating temperature ranges. Tables 3 and 4 show properties of various materials and recommended temperature range. The rotor blade is a critical component for the operation of an FCC unit and is subjected to the greatest stress at high temperatures. The rotor blade will operate approximately 100 to 200°F (38 to 93°C) cooler than the stator blades but due to rotation and centrifugal loading the blade roots will see higher stresses.

Table 3. Showing Materials Used for Blades and Their Typical Mechanical Properties and Temperature Range.

	Waspaloy		Inconel 901	IN 738		A286 (AISI Type 660)
	Room Temp.	1000°F (538°C)	Room Temp.	Room Temp.	1000°F (538°C)	Room Temp.
Tensile min	175	155	170	122	116	130
Yield Strength 0.2% Proof Stress min	120	105	120	96	85	85
Elongation %	15	15	12	7	7	15
Reduction of Area	18	18	15	9	10	20
Inlet Temperature Range	1200 to 1400°F (649 to 760°C)		1100 to 1300°F (593 to 704°C)	1300 to 1500°F (704 to 816°C)		1000 to 1200°F (538 to 649°C)

Table 4. Showing 100,000 Hour Stress Rupture Values.

		Waspaloy	Inconel 901	IN 738	A286 (AISI Type 660)
100,000 Hr. Stress Rupture Values (ksi)	1000°F (538°C)				45
	1100°F (593°C)	64	43		33
	1200°F (649°C)	42	30		22
	1300°F (704°C)	20	15	47	13
	1400°F (760°C)	10		30	
	1500°F (816°C)			18	
	1600°F (871°C)			10.7	

Just like for disks, the melting, forging and heat treatment of these superalloys are important in obtaining the required creep/creep rupture strength with good notch ductility. Both rotating disks and blades are designed for 100,000 hours based upon the smooth bar creep rupture life of the component. In general OEMs apply some appropriate safety factor due to variations of heats of material. In FCC application the factors that can limit the blades life are erosion and/or high temperature corrosion. Both these phenomena will be discussed in the erosion/high temperature corrosion section.

Bolting

OEMs use either a single bolt or a series of bolts for attaching the disk to the shaft. The materials used for the bolts can be Waspaloy, A286, or AISI 422 depending on the disk materials. An important property for the material is the stress relaxation component.

MATERIAL SELECTION FOR NONROTATING EQUIPMENT SUCH AS INLET EXHAUST CASING, STATOR BLADES, BOLTING, ETC.

Inlet/Exhaust Casing

Over the years various materials have been used ranging from 2-1/4 Cr 1 Mo to Hastelloy® X. Table 5 lists temperature range for various casing materials. Today both the inlet and exhaust casing are generally manufactured using AISI 304H or 347/321 materials. Both of these materials are austenitic stainless, which provide good oxidation/corrosion resistance as well as satisfactory creep rupture properties. Figure 11 shows the maximum allowable stress values for 304H, 321H, 347, and 347H ASME Section 1 (ASME, 2007). However, the ductility of these stainless steels can vary considerably as shown in Figure 12. Both the inlet and exhaust casing are fabricated using qualified weld procedures. In general the materials are supplied in a solution treated condition. In the case of AISI 304H, the material is solution treated and water quenched to ensure that the carbon remains in solution. Since AISI 347 or 321 have stabilizing elements, such as titanium or niobium, then the materials after solution treatment are given a stabilizing treatment to precipitate titanium or niobium carbides and suppress the precipitating of chromium carbides at the grain boundaries. Table 6 shows composition of the materials.

Table 5. Temperature Range for Various Casing Materials.

Design Inlet Gas Temperatures			
	1000 – 1200°F (538 - 649°C)	1200 – 1300°F (649 – 704°C)	1300 – 1400°F (704 – 760°C)
Inlet Casing	2-1/4 Cr1Mo	AISI 304H AISI 321/347	AISI 304H Hastalloy AISI 321/347
Exhaust Casing	2-1/4 Cr1Mo	AISI 304H AISI 321/347	AISI 304H AISI 321/347

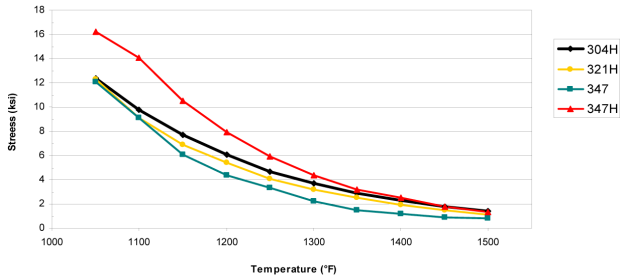

Figure 11. Maximum Allowable Stress Values for 304H, 347, 347H, and 321 ASME Section 1.

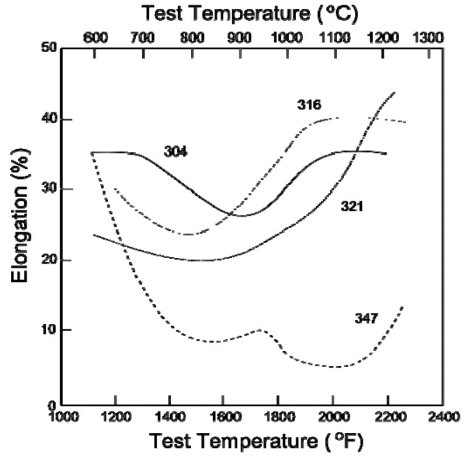

Figure 12. Tensile Ductility of Various Stainless Steels in Short-Time Tests at Elevated Temperatures. (Courtesy Truman and Kirby, et al., 1960)

Table 6. Chemical Composition Requirements, Percent.

UNS Designation	Type	Carbon	Manganese	Phosphorus	Sulfur	Silicon	Chromium	Nickel	Molybdenum	Nitrogen	Copper	Other Elements
Austenitic (Chromium-Nickel) (Chromium-Manganese-Nickel)												
S30409	304H	0.04-0.10	2.00*	0.045*	0.03*	0.75*	18.0-20.0	8.0-10.5	•••	•••	•••	•••
S32100	321	0.08*	2.00*	0.045*	0.03*	0.75*	17.0-19.0	9.0-12.0	•••	•••	•••	Ti 5 X (C+N) min, 0.70 max
S32109	321H	0.04-0.10	2.00*	0.045*	0.03*	0.75*	17.0-19.0	9.0-12.0	•••	•••	•••	Ti 4 X (C+N) min, 0.70 max
S34700	347	0.08*	2.00*	0.045*	0.03*	0.75*	17.0-19.0	9.0-13.0	•••	•••	•••	Cb 10 X C min, 1.00 max
S34709	347H	0.04-0.10	2.00*	0.045*	0.03*	0.75*	17.0-19.0	9.0-13.0	•••	•••	•••	Cb 8 X C min, 1.00 max
note * = maximum												

For both AISI 304 and AISI 321/347, the heat treatment after fabrication (forming/welding) is a stress relief treatment (ASTM, 2008). Since the inlet/exhaust fabrications are complex structures, it is not recommended to apply an accelerated cool down treatment due to possible distortion of the fabrication. Consequently, most OEMs slow cool the stainless fabrication to minimize distortion of the structure and also reduce residual stresses. Consequently, the slow cooling through the sensitizing temperature range 1050 to 1550°F (566 to 843°C) allows for chromium carbide precipitation along the grain boundaries. For OEMs this is less of a concern since during the operation of the FCC unit the stainless steel inlet/exhaust casing materials will precipitate chromium carbide precipitation. Figure 13 shows this phenomenon where 100 percent precipitation can be complete after 10,000 hours (Samians, et al., 1975).

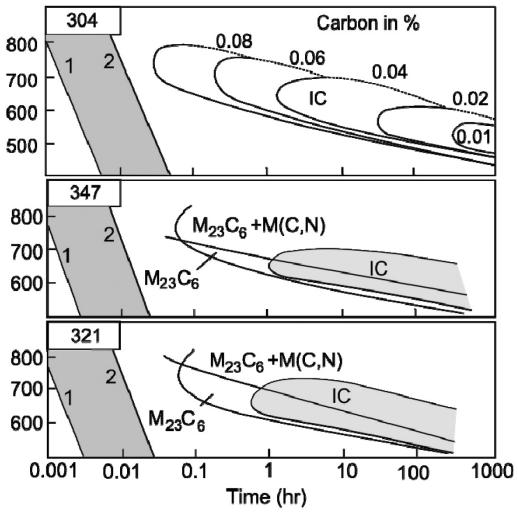

Figure 13. Influence of Structure and Alloying Additions on $M_{23}C_6$ Precipitation and Intergranular Corrosion Attack.

Stainless materials AISI 304H and AISI 321/347 will form the brittle sigma phase during the operation of the unit. Figures 14, 15, and 16 show fabricated inlet and exhaust casings. The formation of the brittle phase sigma after exposure of long times depending on the temperature can significantly affect the materials ductility. Weld repair of inlet and exhaust casings after having been in service can be challenging and certain heat treatments need to be done to improve the weldability. This will be discussed further in the repair section. When comparing the weldability of AISI 304H and AISI 347/321, AISI 304H has far superior crack resistant properties.

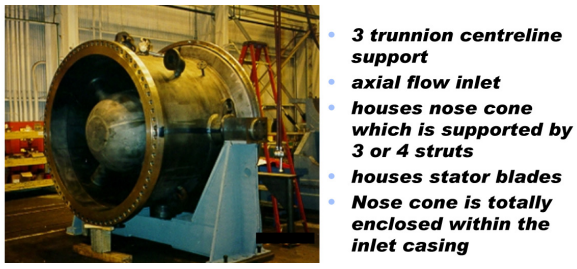

Figure 14. Photo of Expander Inlet Casing.

Table of Contents

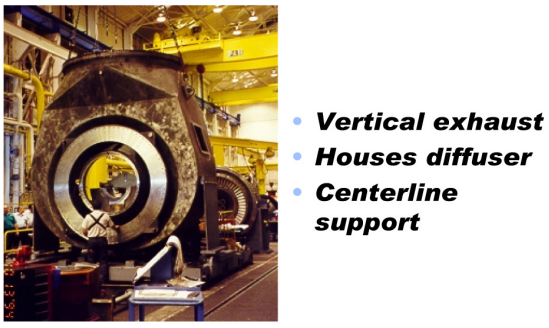

Figure 15. Photo of Expander Exhaust Casing.

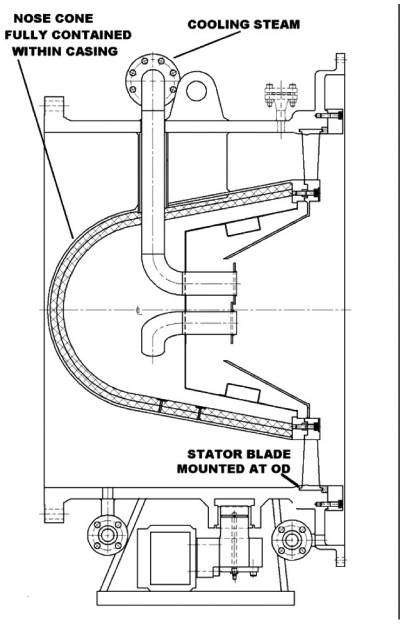

Figure 16. Outline of Expander Inlet Casing.

The authors' company fabricates casing using AISI 304H materials utilizing E308H weld consumables qualified to a controlled delta ferrite range. Processes used are shielded manual arc welding, automatic submerged arc, flux cored arc welding, and gas tungsten arc welding. All the processes have qualified weld procedures in accordance with ASME IX. In the case of AISI 347/321 materials, the weldability is not as crack resistant as the 304H.

During welding or on subsequent heat treatment, the welded AISI 347/321 can be prone to hot cracking. On subsequent heat treatment or during service in the range, 1000 to 1300°F (538 to 704°C), the material can be subject to strain age induced cracking. The presence of NbC can restrict the movement of creep and, subsequently, cause the minute liquation or hot micro cracks to enlarge as unacceptable indications. This cracking mechanism occurs in AISI 347/321 in thicknesses generally over one inch. In 1950/60s, AISI 347/321 heavy wall piping was prone to this form of cracking. Today the stainless steel piping used to transport the hot gas to the expander is generally made from AISI 304H stainless.

Stator Blades

Stator blades in the past have utilized materials such as Waspaloy and Stellite 31. The stator blades upstream of the rotary blades see higher temperatures and, therefore, can be subjected to high temperature corrosion. The Stellite 31 is a cobalt based alloy that has superior oxidation and corrosion than the Waspaloy. All the stator blades whether Waspaloy or Stellite 31 are coated with an erosion resistant coating. The Stellite 31 is a cast material and is processed through stringent quality requirements.

AGGRESSIVE CORROSION AND EROSION ENVIRONMENTS

High Temperature Corrosion

FCC hot gas expanders operate in environments that can be both corrosive and erosive. Although it is well documented that the source of erosion comes from the regenerated catalyst that is carried with the hot flue gas from the FCC, its effect on high temperature corrosion is not well documented.

The nature of corrosive attack is primarily influenced by the type of crude oil stock, which in time has a bearing on the resulting flue gas composition, regenerated catalyst, and the nature and quantity of additives injected into the FCC process.

The regenerator flue gas composition can significantly change depending on whether the regenerator is operated in a complete or partial CO combustion mode (Nieskens, et al., 1990). An example of regenerated flue gas compositions is shown in Table 7.

Table 7. Representative Flue Gas Compositions (mo1% and Associated Equilibrium O_2 and S_2 Partial Pressure.

Gas Components	Partial Combustion	Complete Combustion
N_2	72.0	72.0
CO	7.4	0.04
CO_2	11.2	14.4
H_2O	9.3	11.85
O_2	Trace	1.5
SO_x	0.1	0.21
Equilibrium Partial Pressure*		
$P(O_2)$	$10^{-23.5}$	$10^{-1.9}$
$P(S_2)$	$10^{-8.8}$	$10^{-38.0}$
P(H)	$10^{-11.1}$	$10^{-16.3}$
$P(H_2)$	$10^{-1.45}$	$10^{-11.9}$
$P(H_2S)$	$10^{-3.0}$	$10^{-28.}$
* Calculated equilibrium partial pressures at P = 1 atm, T = 1112°F (600°C)		

Over the years, there have been a number of power recovery turbine blade failures that have occurred in units that operated under a partial combustion mode (for reasons unrelated to erosion, overheating, etc.). Typical flue gas inlet temperatures can range from 1202°F to 1400°F (650°C to 760°C). The fractures investigated have originated in the upper land of the blade root (Figure 17). Subsequent investigations have defined the factors that may give rise to failures in this location. Several important characteristics are noted. One such feature is that relatively thick corrosion products developed in the root section of the blade and disk. These corrosion products primarily comprise Cr_2O_3, CrS, and Ni_3S_2. In addition to being relatively thick, the corrosion products were found to be prone to cracking. As a result of this cracking, growth of the corrosion product into the metal substrate occurred. As described in detail later, the presence of such an oxide penetration acts as if it were a crack in the blade material. It was also observed that the fracture surfaces from the failed components were almost totally intergranular with sharp facet features. This suggests that the blade failed in a manner related to a stress/high temperature corrosion mechanism, i.e., some form of embrittlement effect. Both the blades and rotor disks are fabricated from nickel base alloys (Waspaloy). One important feature that was observed is that the gaps between the blade root and rotor disk were packed with regenerated catalyst residue. Initially it was thought that this catalyst was innocuous. However as will be shown in this tutorial, the regenerated catalyst has a detrimental effect on Waspaloy's fracture toughness.

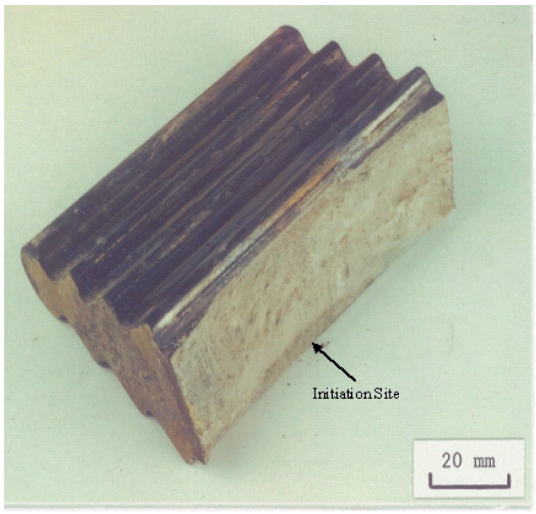

Figure 17. Illustration of an FCC Power Recovery Turbine Blade Failure and Showing Location of Initiation Site (As Indicated by the Arrow).

Corrosion Product Morphology

There are two major differences that occur in blades/disk root sections when exposed to the complete and incomplete combustion conditions. First is the nature of the oxide product that formed in the curved portion of the blade root, adjacent to and above the pressure land. For blades exposed to partially combusted flue gases, a thick stratified corrosion scale is developed that comprises primarily an outer Ni_3S_2 and an inner Cr_2O_3 layer (Figure 18). For a complete combustion mode, the scale comprises primarily Cr_2O_3, with internal precipitates of CrS within the alloy substrate (Figure 19).

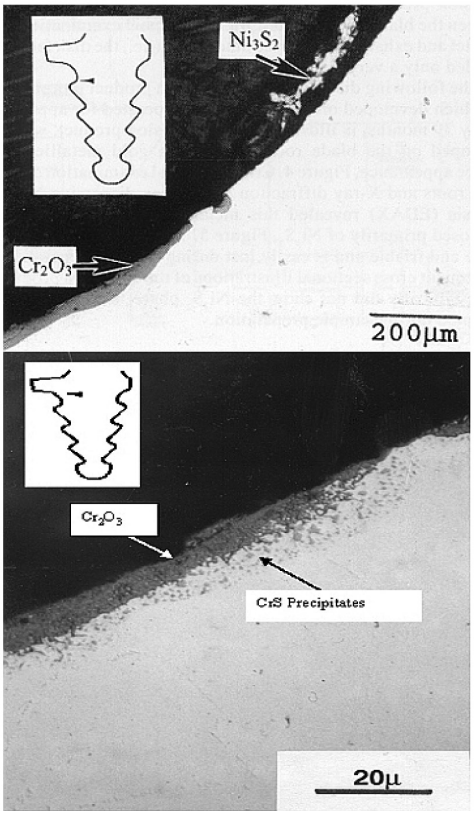

Figure 18. Cross-Sectional Views of the Blade Root in the Curved Area of the First Root Land for a Turbine That Operated with Partial Combustion Flue Gases.

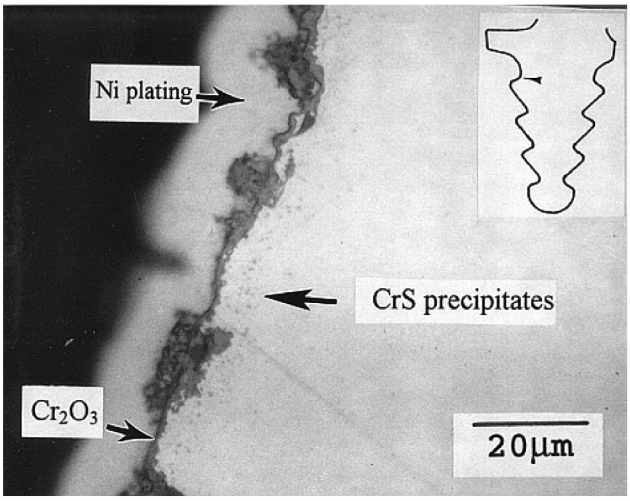

Figure 19. Cross-Sectional View of the Corrosion Product that Developed in the Curved Area of the First Root Land, for a Turbine that Operated with Fully Combusted Flue Gases. Section Was Taken from the Axial Center of the Blade.

The second and perhaps most important difference between the blades exposed to these conditions is the development of an oxide wedge. The formation of an oxide wedge plays a crucial role in the fracture of expander blades. To date, oxide wedges have been observed only on blades exposed to partially combusted flue gases and appears to be related to the thickness of the corrosion product that developed in the curved portion of the root land. For a more detailed description of the morphology (Dowson, et al., 1995).

Oxide Wedges

The failure of blades in service has been found to occur by fracture in the upper root land with initiation on the high pressure side of the blade. The region encompassing the upper pressure land was examined from several intact blades. For units that operated on partially combusted flue gases, one feature of interest found is that related to inward oxide penetration. For the sake of this discussion, this feature is referred to as an "oxide wedge." An example of the shape and location of an oxide wedge is illustrated in Figure 20.

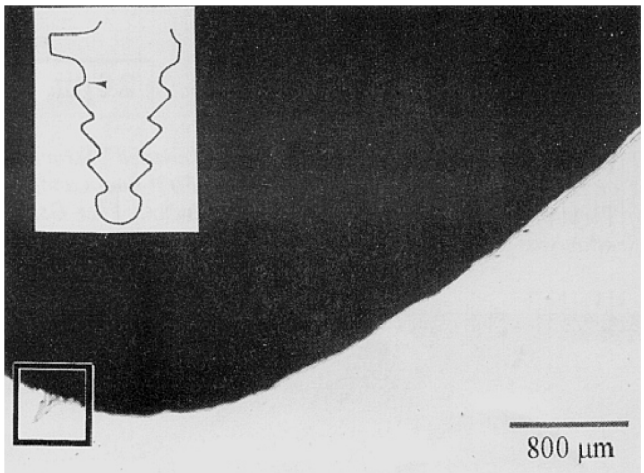

Figure 20. Cross-Sectional View of the Stratified Corrosion Project, and "Oxide Wedge" (In the Highlighted Area) that Developed in the Curved Area of the First Root Land, for a Turbine that Operated with Partially Combusted Flue Gases. Section Was Taken from the Axial Center of the Blade. (Note: The Absence of the Outer Ni_3S_2 Phase Is Due to its Disruption during Blade Disassembly and Sample Preparation).

In Figure 21, an oxide wedge is shown in greater detail, along with X-ray images for Cr, Ni, Co, S and O. It appears that the oxide wedge, for the most part, comprises Cr_2O_3 with the above elements and Ti, Al, and Mo existing in solid solution. The exception is the crack in the oxide wedge center, which is filled with a phase rich in Ni, Co, and S.

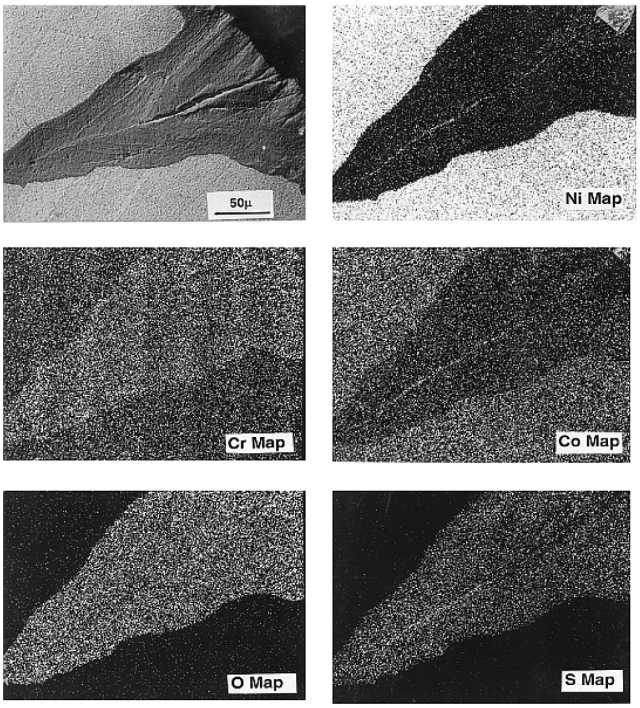

Figure 21. Cross Section SEM Micrograph of the Oxide Wedge Shown in Top Left and the Corresponding X-Ray Images for Cr, Ni, Co, S, and O.

Detailed metallography has been used to determine the size and depth of the oxide wedge penetration, which varies along the length of the blade land. For a given load, the minimum penetration depth occurs near the inlet and exhaust faces of the blade root, whereas the maximum penetration occurs near the axial blade root center. In the case of the oxide wedge shown in Figure 21, which was taken from the axial center of the blade root, the oxide wedge penetrates approximately 280 µm into the blade substrate. The depth of penetration has been found to vary depending upon the magnitude of stress and temperature.

Oxide wedge formation is a form of oxidation/sulfidation damage related to the repeated crack nucleation and growth of the corrosion layer at the oxide wedge tip. The rupture of the corrosion layer at the wedge tip exposes the alloy substrate to the oxide environment. The role of thermomechanical fatigue, creep, and corrosion (and in particular the oxidation damage due to wedge growth) has been examined by Sehitoglu (1992) for steels, Ni-based superalloys, and Al alloys. In a model developed by Sehitoglu (1992) to describe oxide wedge growth, the mechanisms leading to wedge growth incorporated such factors as temperature, strain rate, strain range and strain-temperature phasing.

The Type II oxide intrusion growth, as described by Sehitoglu (1992), appears to approximate the oxide wedge growth observed on the blade roots of power recovery turbines operating with partially combusted flue gases.

In the model developed by Sehitoglu (1992), two strain components contribute to oxide wedge growth; strains associated with mechanical loads and strains due to thermal cycling. Type II oxide growth appears to predominate when the strains associated with the mechanical load and thermal cycling are out of phase, and as the strain component due to thermal cycling approach zero, (i.e., $\Delta T = 0$). Power recovery turbines operate primarily under constant operating conditions, for long periods of time, where the strain components are predominantly due to mechanical loading and not thermal cycling.

Effect of Catalyst

A chemical analysis was performed on catalyst taken from a separator in an FCC unit that operated in a partial combustion state. In addition to the elements associated with catalyst particles, trace amounts of such elemental species as V, Ca, Na, Ni, K, Mg, Ba, Sb and Pb were detected. Elements such as V, Na, and Ca are of concern due their role in deposit-modified (hot) corrosion (Birks and Meier, 1983; Kofstad, 1988). The heavy metals Sb and Pb are of a concern due to their adverse effect on Ni-base superalloy mechanical properties. In addition to the above listed elements, significant amounts of C and S were measured, 0.34 and 0.11 wt percent, respectively.

To assess the role played by the catalyst, samples of regenerated catalyst taken from various expander locations were encapsulated in seamless Waspaloy tubes. One end of the Waspaloy tube was seal welded and the other end was crimped closed. The catalyst-filled Waspaloy tubes were placed in a furnace and heated at 1292°F (700°C) for 120 to 168 hours. A controlled Waspaloy tube with no catalyst present was also placed in a furnace and heated at 1292°F (700°C). A total of eight tubes were tested. After exposure, the tubes were sectioned and examined metallurgically.

The results of the testing showed that with the catalyst present, significant amounts of corrosion (a layer ~ 40 µm thick) were observed. Analysis with X-ray indicated the corrosion product comprises primarily Cr, Ni, O and lesser amounts of S.

Another feature observed was the cracking of the Waspaloy tubing (Figure 22), which was intergranular and exhibited brittle characteristics similar to actual blade failures. It also appeared that the cracking was related to stress, in that the cracks originated from the crimped tube ends and propagated to the tube center. In regions near the tube center where the stresses were low, crack growth was arrested. As a result of these observations, a set of experimental tests were undertaken in an effort to quantify a relationship between stress, temperature, and the onset of cracking in catalyst environments.

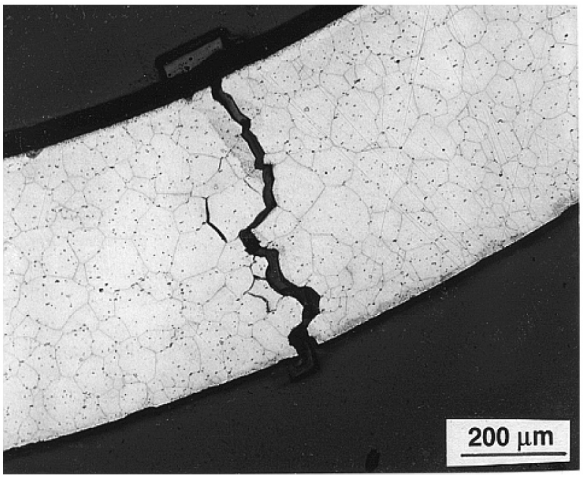

Figure 22. Crack Formation that Occurred in a Waspaloy Tube Filled with Regenerated FCC Catalyst.

High Temperature Mechanical Testing

Stress rupture tests were conducted on notched combination Waspaloy bars under five different sets of "environmental conditions." The results of the tests are shown in Table 8. All tests were conducted from the same heat of AMS 5704, Waspaloy bar (Table 9).

Table 8. Stress Rupture Test Results.

TEST #1 – AS-RECEIVED MATERIAL RESULTS:			
Temperature F (C)	**Stress (MPa)**	**t_f(hr)**	**Location of Failure**
1292 (700)	482	663.3	Smooth Section
1202 (650)	654	931.3	Smooth Section
1112 (600)	757	2667+	Did Not Fail
TEST #2 – S - IMPREGNATED RESULTS:			
Temperature F (C)	**Stress (MPa)**	**t_f(hr)**	**Location of Failure**
1292 (700)	482	259	Smooth Section
1202 (650)	654	350	Smooth Section
1112 (600)	757	346	Smooth Section
TEST #3 – CATALYST "A" FILLED CHAMBER RESULTS:			
Temperature F (C)	**Stress (MPa)**	**t_f(hr)**	**Location of Failure**
1292 (700)	482	0.2	Notch
1292 (700)	482	2.3	Notch
1292 (700)	351	0.9	Notch
1292 (700)	234	334.9+	Did Not Fail
1292 (700)	234	333.6+	Did Not Fail
1202 (650)	654	3.3	Notch
1202 (650)	475	355.6+	Did Not Fail
1112 (600)	757	13	Notch
1112 (600)	757	12.2	Notch
*1022 (550)	137	50.7	Did Not Fail
*Cool down and unload; replenish with new catalyst			
**1022 (550)	137	69.2	Did Not Fail
**Cool down and unload; replenish with new catalyst			
1292 (700)	70	0.3	Notch
TEST #4 – CATALYST "B" FILLED CHAMBER RESULTS:			
Temperature F (C)	**Stress (MPa)**	**t_f(hr)**	**Location of Failure**
1292 (700)	482	70+	Did Not Fail
1292 (700)	550	118+	Did Not Fail
TEST #5 – CATALYST "A" BAKED AT 700°C FOR 8 HOURS, RESULTS:			
Temperature F (C)	**Stress (MPa)**	**t_f(hr)**	**Location of Failure**
1292 (700)	482	119+	Did Not Fail

Table 9. Analysis of Waspaloy Bar (wt%) Used in the High Temperature Mechanical Testing Experiments.

In Weight Percent			
C	0.036	Mn	0.046
S	0.001	Cr	20.11
P	0.010	Si	0.14
Ni	56.88	Mo	3.85
Co	13.15	B	0.005
Fe	1.13	Zr	0.055
Ti	3.11		
PB *5			
In PPM			
*** Not Detected; Number indicates the Minimum Limit of Detection**			

For Test #1, notched combination creep rupture specimens were machined from the as-received Waspaloy bar in accordance with ASTM E292. These bars were directly tested in air atmospheres. For Test #2, the machined specimens were given a sulfur impregnation treatment. This treatment was performed using an evacuated quartz tube, backfilled with argon that contained the notched combination specimen and small amount of sulfur. The sealed quartz tube was then heat treated at 1472°F (800°C) for 100 hr. This treatment resulted in the formation of subsurface CrS precipitates (Figure 23).

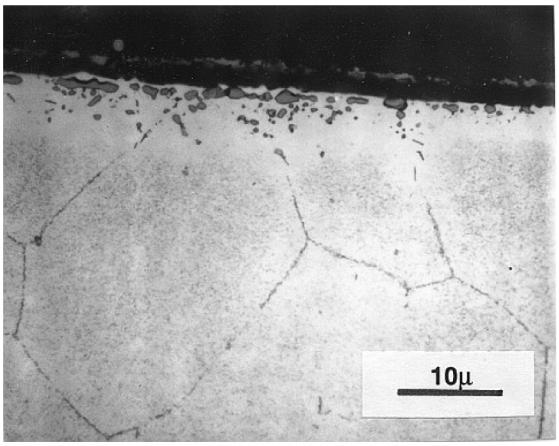

Figure 23. Illustration of Internal CrS Precipitates that Formed in a Waspaloy Coupon Heated in a Quartz Tube, Containing Sulfur at 1472°F (800°C) for 100 Hrs.

For Test #3, a specifically modified creep rupture bar was utilized for insertion into a designed stainless steel chamber (Figure 24) that was filled with 33 gms of regenerated catalyst taken from a partial combustion FCC unit. A quantitative chemical analysis of the catalyst is shown in Table 10. The metallic species present were assumed to exist in the oxide form. A series of modified stress-rupture tests with this catalyst were performed under various load and temperature conditions.

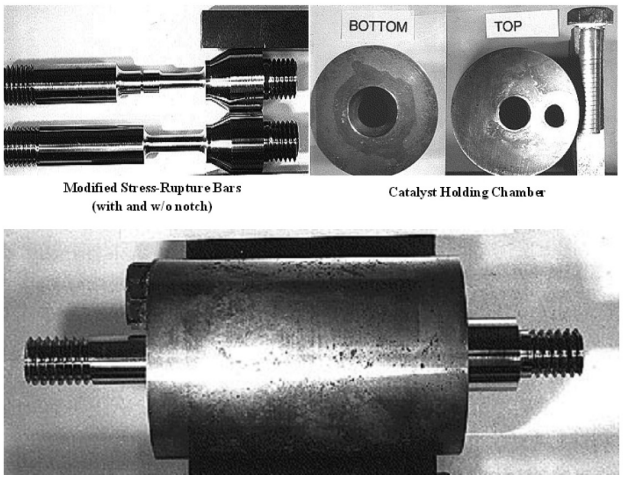

Figure 24. Illustration of the Modified Catalyst Stress-Rupture Test Arrangement with the Catalyst Holding Chamber and Modified Stress-Rupture Bar.

Table 10. Catalyst Used in "Modified Stress-Rupture" Tests (in wt%).

Dry Basis C 0.34 S 0.11			
Other Species			
SiO_2	60.00	NiO	0.19
Al_2O_3	30.66	CaO	0.12
TiO_2	3.95	K_2O	0.12
SrO	2.00	MgO	0.086
Fe_2O_3	0.99	Sb_2O_3	0.067
V_2O_5	0.83	BaO	0.063
Na_2O	0.55	PbO	0.048

Table of Contents

For Test #4, similar tests to Test #3 were done except that the regenerated catalyst was taken from a complete combustion FCC unit.

For Test #5, the catalyst was the same as that used for Test #3, except that the catalyst was prebaked at 1292°F (700°C) for eight hours prior to testing. Analyses of the catalyst before and after baking are shown in Table 11. Two procedures were used to determine the gaseous species being evolved from the heated catalyst through two extraction methods. The first attempt was made by heating the catalyst to 1292°F (700°C) under a flow of nitrogen, passed through a charcoal filter, and the filter washed with solvent to collect any residue. For the second method, the evolved gas was passed through an impinger filled with 10 percent nitric acid in order to capture any metallic compounds. In both cases, the amount of species evolved was too small to detect.

Table 11. Weight Percent of C, S, and H of Partial Combustion Catalyst in the As-Received Condition and after Baking of 1292°F (700°C) for 8 Hours.

	C	S	H
As Received	0.37	0.116	0.21
After Baking	<0.02	0.108	0.1
ICP Scan Metal			
Oxides, Wt%	**As-Received**	**Baked**	
CuO	<.01	<.01	
MgO	.09	.09	
ZnO	<.01	<.01	
Cr_2O_3	<.01	<.01	
NiO	.16	16	
V_2O_5	.70	.71	
CoO	<.01	<.01	
TiO_2	1.9	1.9	
Fe_2O_3	.75	.77	
Al_2O_3	31.4	31.2	
MoO_3	<.01	<.01	
MnO_2	<.01	<.01	
Ce_2O_3	.59	.60	
Na_2O	.36	.36	
BaO	.05	.06	
CaO	.10	.10	
PbO	.02	.02	
As_2O_3	<.01	<.01	
Sb_2O_3	<.01	<.01	
SnO_2	<.01	<.01	
La_2O_3	.33	.33	
K_2O	.13	.11	
Wt. loss due to moisture evolution 0.43%			

Test Results

The stress rupture tests conducted on the as-received and sulfur impregnated specimens found that the specimens failed due to creep. As listed in Table 8, the failure times were typically in the hundreds of hours. In addition, specimens exposed under these conditions did not exhibit notch sensitivity, i.e., all failed in the smooth section of the specimen. In the case of the modified catalyst stress-rupture tests, Test #3, significant and important differences were found. Under these conditions, rapid failure on the order of minutes occurred in the notched section of the specimen. As shown in Figure 25, failure occurred via intergranular crack propagation with sharp facet features.

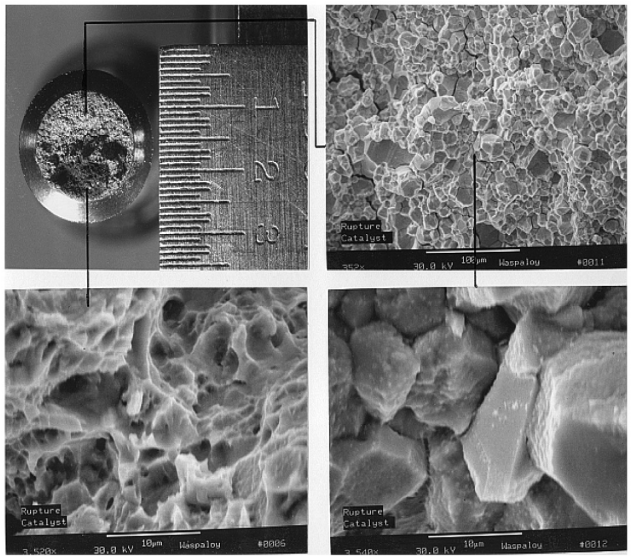

Figure 25. Fracture Surface of a Specimen Tested Under Modified Catalyst Stress-Rupture Test. Exposure Conditions: T = 1292°F (700°C), σ = 482 MPa, t_f = 20 minutes.

Regenerated catalyst taken from a fully combustion FCC unit did not exhibit rapid failure even at higher stress values (Test #4). Also, in the case of Test #5, the baked catalyst did not exhibit rapid failure.

Discussion

Elements such as S, Sb, and Pb are of concern due to their potential deleterious effect on the mechanical properties of Ni-base alloys.

The inability to detect Sb and Pb on the intergranular fracture surfaces would at first suggest that only O and S were the important contributors. However, if sulfur was in fact a major contributor to the rapid fracture, it would be assumed that the specimens that were subjected to S-impregnation would have experienced a similar rapid failure. However, this did not occur. Instead, the effect of S-impregnation appeared to only manifest itself in increasing the amount of creep that occurred.

The rapid fracture of the specimens tested under Test #3, implied that failure occurred as a result of embrittlement or high temperature stress corrosion cracking (HTSCC). As compared to steels and stainless steels, Ni-base alloys generally exhibit improved resistance to environmental embrittlement (Kolts, 1987). However, under combined specific environmental conditions and tensile stresses, Ni-base alloys can exhibit environmentally induced embrittlement. This embrittlement is thought to occur by either stress corrosion cracking (SCC) or hydrogen embrittlement.

Although the exact mechanism was not truly identified, an important point raised from these tests is that a catalyst environment can induce rapid failure of Waspaloy specimens. Since the catalyst residue is found packed between the blade root and disk, similar conditions may exist in an actual operating power recovery turbine whereby environmentally assisted fracture is possible.

When viewed in the context of fracture mechanics, it can also be inferred that in catalyst environments, the fracture toughness of Waspaloy, MPa $m^{½}$, is significantly reduced. Consequently, the critical plane-strain stress intensity factor value for which subcritical crack growth in a material statically loaded in an aggressive environment is designated $K_{I,HTSCC}$. As will be shown in the next section, a value of $K_{I,HTSCC}$ can be extracted from the data generated from Test #3 results. The relevance and importance of the derived value of $K_{I,HTSCC}$ will, furthermore, be demonstrated in the fracture mechanics model that was derived to explain the failures of blades that had formed oxide wedges.

Fracture Mechanics Model

As mentioned, blades that have experienced failure in the root land have been found to contain oxide wedges. The existence of an oxide wedge is expected to act as a stress concentrator. In fact, the oxide wedge itself can be taken as a flaw or crack within the blade substrate material. When viewed in the context of fracture mechanics, a stress-intensity factor can be calculated at the oxide wedge front. The magnitude of the stress intensity is a function of both the oxide wedge shape and depth, as well as the applied stress acting perpendicular to the oxide wedge propagation direction.

In addition to oxide wedge formation, the accumulation of catalyst residue within the gap between the blade root and disk is also expected to play an important role. As described in the previous section, Waspaloy, in the presence of catalyst debris, experiences rapid brittle fracture. From a fracture mechanics viewpoint, this can be looked upon as a reduction in the fracture toughness of Waspaloy.

A model, based on fracture mechanics, is proposed that incorporates both the effects of oxide wedge formation and the apparent reduction in fracture toughness of Waspaloy in contact with catalyst residue.

Stress Intensity

Due to the fact that a uniform stress field does not exist in the root land under consideration (in the vicinity of the oxide wedge), an assessment of the stress intensity, ahead of an oxide wedge, was performed utilizing the method of weight functions. The weight function method has proven to be a useful and versatile method for calculating stress intensity factors. This is especially true for cracks subjected to nonuniform stress fields, including cracks in weldments or cracks under thermal loading (Xu and Carlsson, 1991; Glinka and Shen, 1991; Shen and Glinka, 1991).

A stress intensity factor can be calculated by integrating the weight function m(x, a) and the stress distribution $\sigma(\chi)$ acting in the prospective crack plane. This results in the following expression for the stress intensity factor (K_I).

$$K_I = \int_o^a \sigma(x) m(x,a) dx \qquad (1)$$

The determination of the weight function m(x,a) requires a complex elastic analysis of the cracked body. As found in the literature, a number of weight function solutions exist for cracks in different geometric bodies and configurations (e.g., surface elliptic cracks in a finite body, edge cracks in a semi-infinite plate, etc.) (Xu and Carlsson, 1991; Glinka and Shen, 1991; Shen and Glinka, 1991).

In the following discussion, the weight function utilized in calculating the stress intensity at the oxide wedge tip was obtained from Glinka and Shen (1991) for an edge crack in a semi-infinite plate. The use of the weight function for such a geometry is deemed appropriate due to conservatively higher values of stress intensities obtained.

The weight function utilized was Equation (2):

$$m(x,a) = \frac{2}{\sqrt{[2\pi(a-x)]}}\left(1 + 0.5693\left(1 - \frac{x}{a}\right) + 0.279375\left(1 - \left(\frac{x}{a}\right)^2\right)\right) \qquad (2)$$

In this equation, "a" is the oxide wedge depth, and "x" is the coordinate dimension, in the x direction, which contains the oxide wedge.

The stress field $\sigma(\chi)$ has to be determined for an uncracked body using an analytical, numerical, or experimental method of stress analysis. In the case of an expander blade, the stress distribution, in the vicinity of an oxide wedge, was obtained through a finite element analysis. From this stress profile, an analytic equation representing stress as a function of distance into the blade root, x, can be obtained, $\sigma(\chi)$. Integrating the product of the stress distribution $\sigma(\chi)$ with the appropriate weight function, Equation (2), results in the stress intensity at the tip of the oxide wedge. The results of such an integration can be represented in a plot of stress intensity, K_I, versus oxide wedge depth (Figure 26).

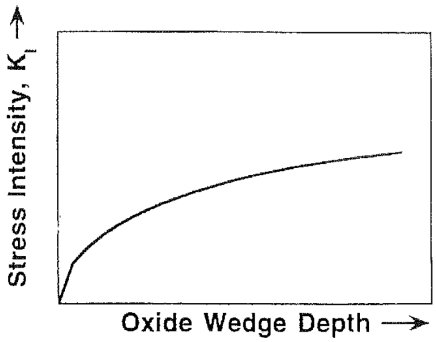

Figure 26. Stress Intensity Profile, as a Function of Oxide Wedge Depth Penetration into the Blade Root Substrate.

Fracture Toughness

As discussed earlier, testing of the modified stress-rupture bars, in contact with regenerated FCC catalyst, resulted in rapid brittle intergranular specimen failures. Failure times were typically on the order of minutes. Assuming that specimens tested by the modified stress-rupture test exhibited brittle fracture, use may be made of the analytical relationships that have been developed for a notched specimen in the determination of a stress intensity factor. Although a rigorous determination of a material's fracture toughness was not possible, it is felt that a bounding value of a material's fracture toughness, K_{IC}, may nonetheless be obtained. In that these values were obtained under aggressive environments, the fracture toughness may more appropriately be described as $K_{I,HTSCC}$.

It has been shown (Sih, 1965) that the stress intensity, K_I, for a notched circular bar can be calculated. The stress intensity is a function of the applied stress and both the notch and bar diameters. Based on this analysis, the stress intensities for notched bars tested with catalyst can be calculated. Under the various loadings tested, there appeared to be maximum stress intensity, above which the modified notch combination bars failed in a rapid brittle mode. For the purposes of this discussion, the critical stress intensity will be referred to as $K_{I,HTSCC}$. The value of $K_{I,HTSCC}$ tested in the presence of catalyst is significantly less than the value of K_{IC}, 110 MPa $m^{1/2}$ measured for unexposed Waspaloy at elevated temperatures. It is important to recognize that the value of $K_{I,HTSCC}$ can be treated as a material property. That is, the fracture toughness determined for Waspaloy under catalyst corrosion tests can be applied to other geometries and loading conditions. When the value of $K_{I,HTSCC}$ is superimposed on the plot for stress intensity versus oxide wedge depth, Figure 27, it has been found that for blades that have failed, the applied stress intensity either equals or exceeds $K_{I,HTSCC}$. Conversely, for blades that did *not* fail and yet contained oxide wedges, the stress intensities of the oxide wedge were found to be *less* than $K_{I,HTSCC}$.

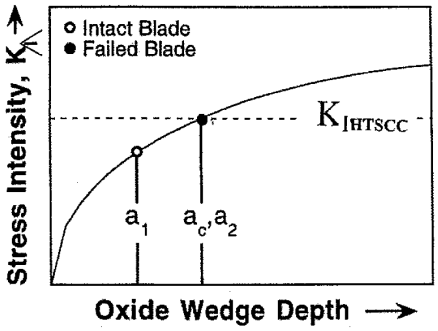

Figure 27. Stress Intensity Profile Versus Oxide Wedge Depth for Unit A. Critical Oxide Wedge Depth for Failure Was Defined as a_c. In the Failed Blade, a_2 Was Found to Exceed a_c. In an Intact Blade, a_1 Was Less Than a_c.

The results of such an analysis were obtained from three separate units. In Figure 27, two blades from the same unit were compared: one intact and one failed blade. The results from the three units confirm the validity of the model.

The above analysis does not imply that rapid, instantaneous failure occurs when the K_I at the oxide wedge tip exceeds $K_{I,HTSCC}$. It is instead envisioned that under actual conditions, a likely failure scenario involves the local environment adversely reducing Waspaloy's fracture toughness in the region ahead of the oxide wedge. Once the toughness has been reduced below $K_{I,HTSCC}$, an intergranular crack initiates and grows. The crack will then grow until it encounters material within the blade root that has a higher fracture toughness; at that point crack growth is arrested. Given time, the local environment will again lower the fracture toughness ahead of the crack. When the fracture toughness is less than $K_{I,HTSCC}$, crack growth will resume. This process is expected to be repeated until total blade failure occurs. It is also important to recognize that as the crack increases in size, the stress intensity ahead of the crack also increases. Thus the crack, in effect, can grow into "tougher" material.

Protective Measures

As a result of the blade failures described, several approaches were taken to resolve the problem. These include steam barrier system, diffused chromium enrichment, plasma sprayed disk root coating, and a new corrosion resistant superalloy.

Steam Barrier System

The preventive measure that is presently being used by the authors' company is the steam barrier system. This system has been successfully incorporated into a unit that has been in operation for well over four years. The principle behind the steam barrier design is to inject steam into the inlet and exhaust chambers to prevent the ingress of gas and catalyst into the disk/blade root area. Also, the large quantities of steam cool the disk/blade roots to a temperature of less than 842°F (450°C), where high temperature corrosion is minimized. In such an approach, the potential for high temperature corrosion can be greatly reduced or eliminated. The theory and sealing flow requirements for a shrouded, rotating disk with external swirling flow have been described (Izenson, et al., 1994). The steam barrier system has already been implemented and has been proven to be a preventive measure against high temperature corrosion.

Diffused Chromium Enrichment

Another prevention method is the application of a coating to the blade/disk root area to prevent or greatly reduce the potential for high temperature corrosion. The application of coatings has enabled the use and life extension of components exposed to harsh, oxide environments.

Chromium and aluminum-rich coatings are used to improve the oxidation resistance of iron and nickel base superalloys. Although coatings offer a means of achieving or improving the corrosion resistance behavior of a material, drawbacks can exist. For instance, the creation of a new surface or interface can lead to other problems, such as fatigue crack initiation sites.

Due to the improved resistance to sulfidizing attack and inherent ductility, the application of a chromium rich coating was developed. An additional objective was to achieve an increase in the surface activity of chromium in the alloy without the formation of an interface between the coating and the metallic substrate. By raising the surface activity of chromium, this results in effectively shifting the kinetic boundary (KB), shown in Figure 28, to the left, and thus promoting the formation of a protective Cr_2O_3 layer. The kinetic boundary is defined as the O_2 partial pressure necessary for a continuous Cr_2O_3 layer to develop on an alloy surface. Typically, this is 10^2 to 10^3 times higher than the Cr_2O_3 to CrS equilibrium values (Xu, et al., 1994; Xu, et al., 1993). The formation, however, of an outer alpha-chromium layer is undesirable, in that such a layer is brittle and prone to cracking. It is important that this layer be removed after the chromizing treatment.

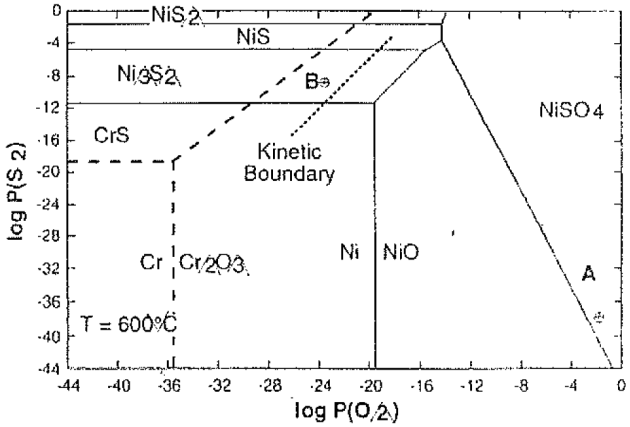

Figure 28. Superimposed Thermodynamic Stability Diagrams for the Ni, Cr, S, and O Systems at 1112°F (600°C). Point A Corresponds to an "Oxidizing" Environment Typical of Fully Combusted Flue Gases. Point B Corresponds to a "Sulfidizing" Environment Typical of Partially Combusted Flue Gases.

To achieve the desired coating composition, the pack cementation process was selected. Figure 29 illustrates the chromium composition of a chromized Waspaloy sample. Corrosion testing has shown that chromized Waspaloy exhibits a 100-fold decrease in the amount of oxide/sulfide attack (as indicated by weight gain measurements) when compared to uncoated Waspaloy. Metallographic examination confirmed the existence of a protective Cr_2O_3 scale. By increasing the corrosion resistance, the formation and subsequent thickness of a stratified corrosion product layer, which in turn results in oxide wedge formation, is reduced as compared to nonchromized Waspaloy.

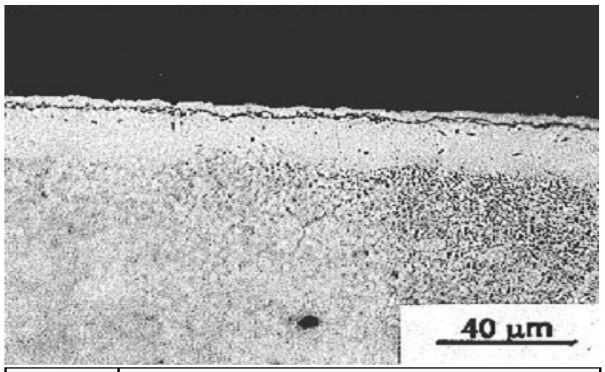

Distance from Surface, Microns	Weight %						
	Al	Ti	Cr	Fe	Ni	Co	Mo
2	0.3	0.2	84.8	3.0	6.1	1.6	3.9
5	1.4	1.0	33.7	7.4	REM	10.9	2.9
8	0.3	0.3	32.7	7.2	REM	11.2	3.0
11	0.7	5.5	29.3	6.4	REM	10.4	2.9
14	0.7	0.8	28.1	5.6	REM	11.8	2.9
17	0.9	1.3	26.8	5.3	REM	11.3	3.0
20	0.8	1.3	25.8	4.2	REM	12.1	3.2
23	1.2	1.7	24.6	3.6	REM	11.9	3.6
26	1.3	2.1	23.2	3.2	REM	12.2	3.3
29	1.3	2.3	21.7	2.8	REM	12.4	3.3
32	1.5	2.7	21.3	2.7	REM	12.6	3.2
35	1.4	1.9	22.1	1.9	REM	14.3	3.9

Figure 29. Illustration of Chromized Layer on Waspaloy.

Numerous tests were done to develop the optimum diffused coating and operational parameters to achieve the desired surface chemistry. This aspect of the development was critical since the objective is to diffuse chromium into the alloy without the

formation of any detrimental phases. These phases can adversely affect the high temperature corrosion resistance of the coated Waspaloy and, in certain cases, drastically affect the mechanical integrity of the rotating Waspaloy components. The chromized coating development has been completed and actual coated blades have been in operation for more than three years without any high temperature corrosive attack.

Plasma Sprayed Disk Root Coating

Although coating of blades can be achieved without detrimental dimensional changes, the disks for larger hot gas expanders present a more difficult challenge. For this reason, application of a plasma sprayed coating at the upper radius portion of the disk roots was developed.

High temperature corrosion tests were run where both coated and noncoated Waspaloy samples were tested under highly sulfidizing conditions. The plasma spray coated Waspaloy samples were found to successfully prevent corrosion of the Waspaloy substrate and exhibit a tenfold decrease in oxidation rate compared to uncoated Waspaloy (as indicated by weight gain measurements). Again, the purpose of the coating was to minimize the formation of an oxide wedge at the high stress intensity locations. Although plasma sprayed coatings are known to crack under thermal cycling, power recovery turbines operate primarily under constant operating conditions for long periods of time. Consequently, the strain components are predominantly due to mechanical loading.

New Corrosion Resistant Superalloy

Since chromizing of large disks is extremely difficult, development of the new superalloy was instigated and is now complete and available for implementation. The high temperature corrosion tests of the new alloy under highly sulfidizing conditions were found to exhibit a twofold decrease in the amount of oxide attack as compared to Waspaloy. The high temperature mechanical properties of the new alloy compared favorably with that of Waspaloy (Yakuwa, et al., 1998).

CORROSION

On cooling during shut down of the FCC unit, polythionic acids can form and attack austenitic stainless steel components leading to stress corrosion cracking to occur. The FeC forms on the stainless steel on account of the H_2S and on cooling after shut down it reacts with water and air to produce the polythionic acids. The polythionic acid attacks Cr-defected zones that are formed at grain boundaries in sensitized parts. The sensitization can occur either during service or during the manufacture of the component. For austenitic stainless steel materials, such as AISI 304H, AISI 347 and AISI 321, when exposed at temperature greater than 850°F (454°C) for long times will lead to sensitization.

There are procedures that can be applied during a shut down for a normal turnaround inspection and repair. See APPENDIX A, which outlines a typical procedure that can be applied.

EROSION ENVIRONMENTS

Erosion of expander components is generally caused by the catalyst particles that flow in the hot gas stream. The impact of the erosive particle on the blade erode the blade in various patterns depending on various factors:

- Angle of attack
- Velocity of blade
- Temperature excursions
- Catalyst type
- Particle size and concentration

Primary erosion is caused by large particles greater than 10 µm. Generally good separators performance and limited gas velocities together with a hard face coating on this part of the blade will confront this type of erosion. Figures 30, 31, and 32 show various types of primary erosion on both stator and rotating blades.

Figure 30. Primary Erosion of a Stator Blade.

Figure 31. Primary Erosion of Rotating Blades (A).

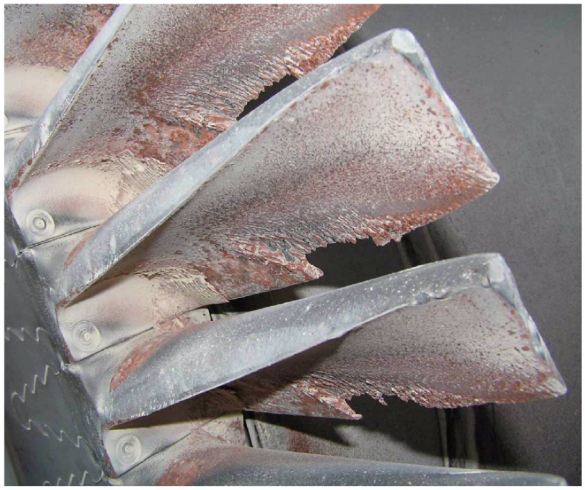

Figure 32. Primary Erosion of Rotating Blades (B).

Another type of erosion is secondary erosion. This phenomenon is caused by small particles that cannot be removed by the separators. Figures 33 and 34 show evidence of secondary erosion.

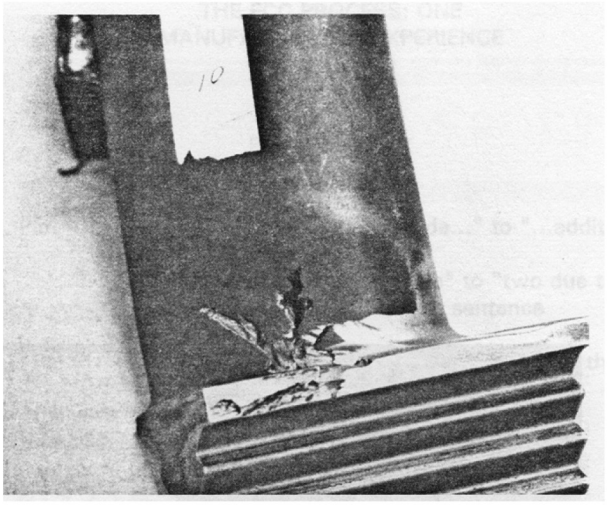

Figure 33. Secondary Erosion of Waspaloy Rotating Blades (A).

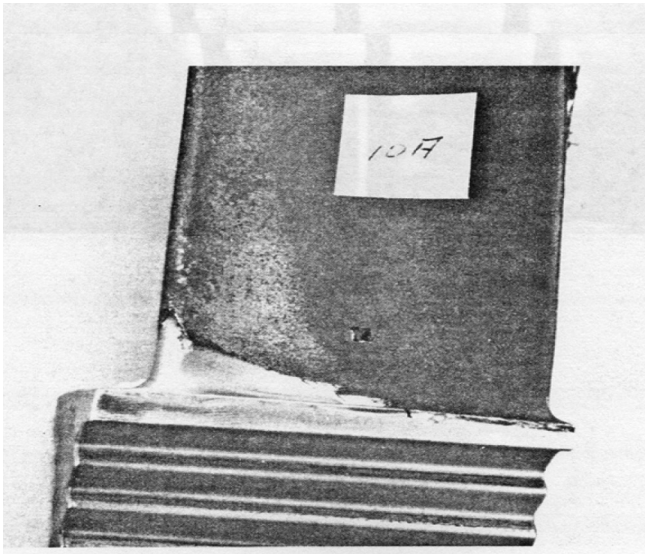

Figure 34. Secondary Erosion of Waspaloy Rotating Blades (B).

Through the years significantly technological advances have allowed for the application of computational fluid dynamics (CFD) and laboratory testing in erosion/temperature map. By utilizing these tools together with results from the field, design enhancements have led to streamlining the air flow between the stator blades and rotating blades. Both these components are coated with erosion resistant coatings using various processes such as detonation gun (D-gun), super D-gun, and high velocity oxy fuel (HVOF).

Extensive erosion testing done by the authors' company showed that Cr_3C_2 coating was the most useful as compared to the WC. The matrix for the Cr_3C_2 is 80 per cent nickel/20 per cent chromium and for WC 75 chromium 25 nickel. Also the Cr_3C_2 shows a closer match of expansion coefficient with the actual blade materials. Its oxidation resistance is better than WC and its resistance to solid particle erosion is good. Less effective as the curves indicates is WC (Figure 35). Although WC coating was applied in the 70s and early 80s with some success, the Cr_3C_2 coating is typically the coating that is applied today. Spalling due to differential thermal expansion can occur and was more evident on blades coated with WC coatings. Table 12 shows thermal expansion coefficient of base material and coatings and the degree of mismatch supplies have suggested that a mismatch less than 3.5×10^3 inch/inch (m/m) is desirable (Sturley, et al., 1981).

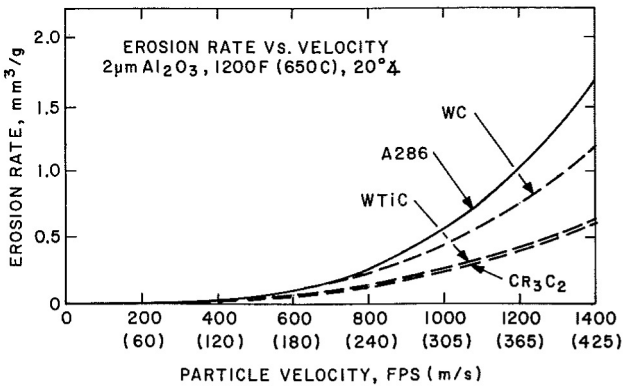

Figure 35. Solid Particle Erosion of Various Coating Materials.

Table 12. Thermal Expansion.

Identification	Temperature Range F(C)	Coefficient of Thermal Expansion a x 10^{-6} in/in°F (x 1.8 m/m°C)
A286	70-1050 (20-565)	9.9
Waspaloy	70-1200 (20-650)	8.0
Waspaloy	70-1400 (20-760)	8.5
403	70-1200 (20-650)	6.5
Cr_3C_2	70-1200 (20-650)	6.1
WC	1400 (760)	4.6
WTiC	400 (250)	4.4
Co	70-1200 (20-650)	8.6
Co-Cr_3C_2	-----	-----
Mismatch of Thermal Expansion		
Identification Coating/Basis Metal	**Temperature F(C)**	**Mismatch a x 10^{-3} in/in (m/m)**
Cr_3C_2/A286	1050 (565)	3.7
Cr_3C_2/Waspaloy	1200 (650)	2.15
WC/A286	1050 (565)	5.2
WC/Waspaloy	1200 (650)	3.8
WC/Waspaloy	1400 (760)	5.2

By steamlining the gas flow between the stator blades and rotating blades, secondary erosion is eliminated (Figure 36).

Figure 36. Rotating Waspaloy Blades after Nine Years Continuous Service.

In addition to erosion caused by the catalyst, the catalyst can adhere and deposit in the flow path. Build up of catalyst on the shroud can cause rubbing of the rotating blades and lead to material removal from the blade tips. Excessive blade tip rubbing can lead to radial blade tip cracking due to excessive heat build up (Figures 37, 38, and 39). Along with material removal caused by the catalyst deposits can lead to a drop in efficiency.

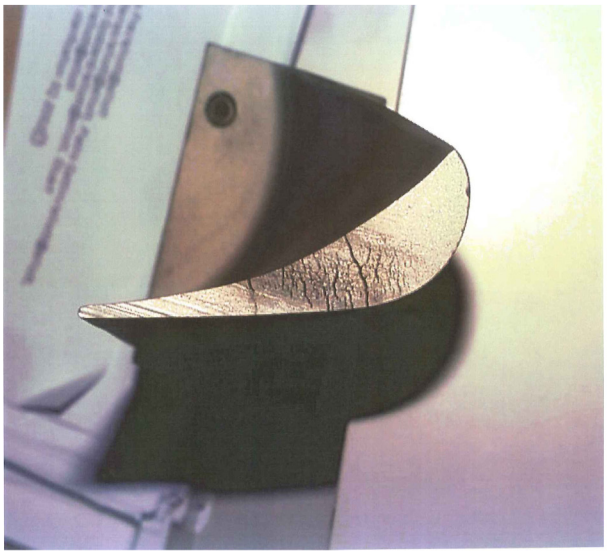

Figure 37. Blade Tip Cracking on Waspaloy Rubbing Against Catalyst.

Figure 38. Rub Tip Cracking on Rotating Waspaloy Blade Leading to Material Removal.

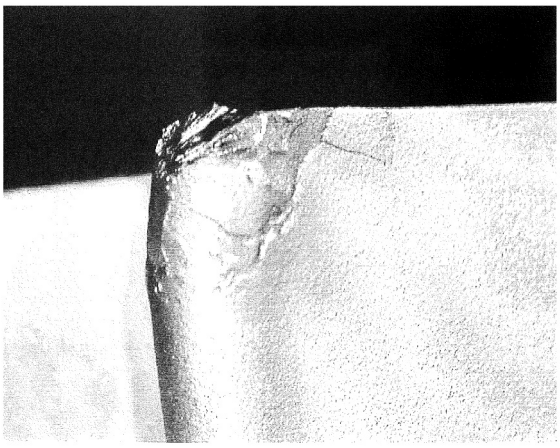

Figure 39. Slight Catalyst Erosion on Tip of Rotating Waspaloy Blade.

REPAIRS OF COSTLY TO REPLACE/ DELIVERY OF COMPONENTS SUCH AS TURBINE DISKS, BLADES, INLET/ EXHAUST CASING, AND STATOR BLADES

In the rotating equipment industry, service of components requires either replacement with new or refurbishment of the components. The refurbishment can mean restore the component to its original dimension either by welding/mechanical fix or other sprayed/plating processes. Most OEMs have developed repair procedures for most of the long lead delivery components, i.e., components such as rotating blades, inlet/exhaust casing, stator blades and shroud ring.

Unlike rotors for compressors and steam turbines, expander rotors have only successfully applied repair by welding to rotor blades. Weld repairs to the disks made from either Waspaloy or A286 has not been done successfully. When a disk failure has occurred, the damage has been so vast that repairs by welding would be unacceptable (Figure 40 and Figure 41). Failures of disks by either high temperature corrosion or overheating caused by a catalyst rub would require matching filler weld composition and the required creep rupture properties of the parent material. Weld repairs of both Waspaloy and A286 are prone to liquation type cracking and, therefore, can only be applied in low stress locations. Figure 42 shows liquation type cracking in the heat affected zone of Waspaloy.

Figure 40. Photograph of Failed First Stage Disk. Arrows Indicate Area Where Disk Tenons Remained Attached.

Table of Contents

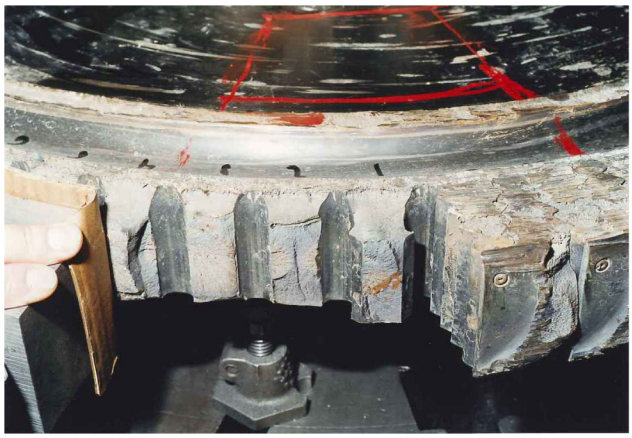

Figure 41. Photograph of Failed First Stage Disk Illustrating Fractured and Intact Disk Tenons.

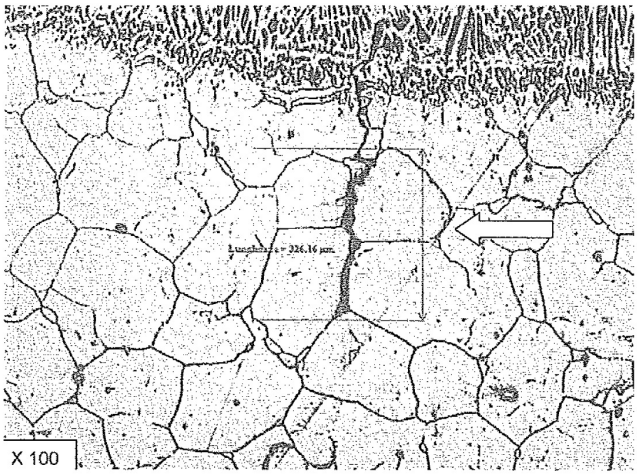

Figure 42. Liquation Type Cracking in HAZ Waspaloy Weld Build Up.

However, rotating blades have been successfully weld repaired in the upper section of the airfoil and on the platform of the blade root. As stated, previously the repairs are done in those areas of low stress. To the authors' knowledge, no weld repairs have been done at the root section or lower section of the airfoil. Generally the repairs have been applied at the airfoil tips where damage was due to rubbing against catalyst buildup on the stationary shroud (Figure 43). Most OEMs have developed qualified weld repairs procedures for repairing either Waspaloy or A286 blades.

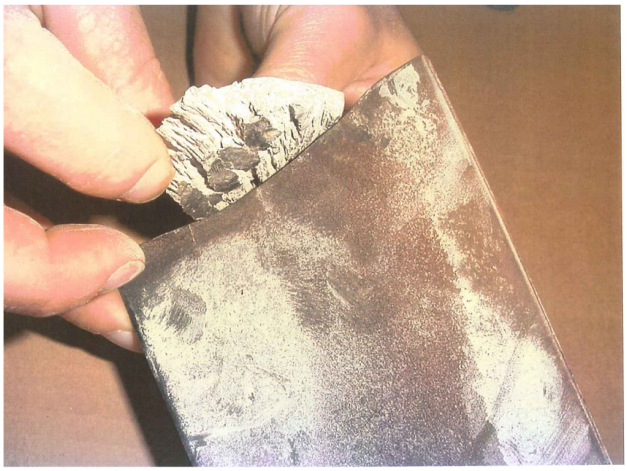

Figure 43. Erosion Damage on Tip of Waspaloy Blade Due to Catalyst.

For stator blades or stationary blades manufactured from Waspaloy AISI 685 materials, the weld repairs procedures applied are similar to that for rotating blades. Generally, if the stator blades are damaged extensively, then replacement blades are purchased.

At the higher operating temperatures stator blades are made from cast Stellite 31 material, which is a cobalt base material and, therefore, has improved oxidation and high temperature corrosion resistance as compared to nickel base alloys. As for Waspaloy, qualified weld repair procedures are developed by OEMs to ensure that the optimum high temperature properties are applied.

In the case for inlet/exhaust casings, weld repairs are applied to ensure the functionality of the machine. If the machine has an extensive number of operating hours, then the casing may be processed through a solution treatment procedure. Whether the material is AISI 304 or AISI 347/321H overtime in excess of 20 to 30 thousand hours, an embrittlement phase called sigma phase will precipitate from the delta ferrite (generally at the grain boundaries). This brittle phase reduces the ductility of the material and can lead to cracking due to a thermal excursion or on startup. The re-solution heat treatment does not remove the sigma phase but after re-solution, the material forms new grain boundaries and the remaining sigma phase is now within the austenite matrix instead of at the grain boundaries.

REMAINING LIFE ASSESSMENT OF HOT GAS EXPANDER COMPONENTS

Introduction

In recent years more and more expanders are reaching their initial design life and there is a need to evaluate the remaining life of critical components. In today's market there is a strong desire to continue operating past the design life of the expander. Questions bearing in managers' minds are what is the machine condition and whether they can be continually operated (if yes, how long). The answer is significant not only for safety concerns but also for cost reduction, especially with today's limited budgets. Therefore, there is an increasingly strong desire for the engineering aftermarket service to perform "remaining life assessment" of hot gas expanders.

A remaining life assessment is the use of technological techniques to predict the remaining life of structures and components that have reached or exceeded their design life. Remaining life assessment is an on going process and not a one time event. Therefore, a remaining life assessment study of 20 years does not mean 20 more years till next inspection.

Remaining life assessment is to use metallurgical and fracture mechanics methodologies to predict the remaining life of structures and components that have been in service for an extended period of time, usually close to or beyond the designed life. Traditionally, if parts are found with material degradations or damages during an overhaul, they might be scrapped and replaced for risk-free consideration, even though they might have some useful life. Remaining life assessment offers a possible tool to estimate the useful remaining lifetime and avoid premature scrapping of the parts. So remaining life assessment is considered to be an attractive method/process for cost reduction and reduction downtime.

Remaining life assessment has often been improperly referred as "life extension." Actually this analysis cannot extend the lifetime of the components. It can only assess the useful remaining lifetime, based on the metallurgical examinations and theoretical (fracture mechanics) calculations. If such assessments indicate the need for extensive replacements and refurbishments, life extension may not prove to be a viable option. Above and beyond this objective, remaining life assessment technology serves many other purposes. It helps in setting up proper inspection schedules, maintenance procedures and operating procedures. It should, therefore, be recognized at the outset that development of techniques for

remaining life assessment is more enduring in value and broader in purpose than simply the extension of plant life. For instance, it has been possible to extend the inspections from two to six years for modern rotors, on the basis of assessments based on fracture mechanics, resulting in considerable savings.

In implementing remaining life assessment procedures, the appropriate failure definition applicable to a given situation must be determined at the outset, and the purpose for which the assessment is being carried out must be kept in mind. While determining the feasibility of extended plant life may be one objective, a more common objective is the setting of appropriate intervals for inspection, repair and maintenance. In this context, remaining life assessment procedures are used only to ascertain that failures will not occur between such intervals. It should never be assumed that having performed a remaining life assessment study for a 20-year life extension, one could then wait for 20 years without interim monitoring. Periodic checks to ensure the validity of the initial approach are essential. In this sense, remaining life assessment should be viewed as an ongoing task, rather than a one-time activity.

A phased approach, in which the initial level includes nonincursive techniques followed by other levels of actual plant monitoring, then followed by nondestructive inspections and destructive tests would be the most logical and cost-effective approach. In Level I, assessments are performed using plant records, design stresses and temperatures, and minimum values of material properties from the OEM. Level II involves actual measurements of dimensions, temperatures, simplified stress calculations and inspections coupled with the use of minimum material properties from the OEM. Level III involves in-depth inspection, stress levels, plant monitoring, and generation of actual material data from samples removed from the component (destructive testing). The degree of the detail and accuracy of the results increases from Level I to Level III, but at the same time, the cost of the assessment also increases. Depending on the extent of the information available and the results obtained, the analysis may stop at any level or proceed to the next level as necessary.

In order to evaluate the remaining life of expander components, one needs to understand the mechanisms in which failure can occur. In expander components, the remaining life is governed by one or more of the following failure mechanisms:

- High temperature creep
- Fatigue—high cycle or low cycle
- Erosion—catalyst
- High temperature corrosion/embrittlement
- Embrittlement

However, in remaining life assessment, usually only those mechanisms depending on temperature & time are taken into account. For example, for turbine casing, engineers usually focus on thermal-stress induced low cycle fatigue, creep rupture, and tempering embrittlement cracking. These failures usually are slow processes, therefore, can be assessed and forecasted by examining the warning evidences in the material.

Countless works have been done to study the behaviors of fatigue crack initiation/propagation and creep or embrittlement rupture in materials. Scientists and engineers have reached to such a level that, by knowing the flaw size or microstructure deterioration/damage, one can theoretically calculate and predict the remaining lifetime of the parts, based on the knowledge of the material properties and understanding of the stress distributions.

Fatigue

Failures that occur under cyclic loading are termed fatigue failures. These can be vibration stresses on blades, alternating bending loads on shafts, fluctuating thermal stresses during start-stop cycles, etc. There are two types of fatigue: low cycle fatigue (LCF), high cycle fatigue (HCF). Traditionally, low cycle fatigue failure is classified occurring below 10^4 cycles, and high cycle fatigue is above that number. An important distinction between HCF and LCF is that in HCF most of the fatigue life is spent in crack initiation, whereas in LCF most of the life is spent in crack propagation because cracks are found to initiate within 3 to 10 percent of the fatigue life. HCF is usually associated with lower stress, while LCF usually occurs under higher stress.

Remaining life of expander casings or its rotating components is generally based upon crack growth consideration. Fracture mechanics is the mathematical tool that is employed. It provides the concepts and equations used to determine how cracks grow and their effect on the strength of the structure. At the authors' company fracture mechanics is utilized in analyzing the structural integrity of components that have been in operation to determine whether the component is suitable for further operation. Based upon crack growth analysis one considers a number of scenarios.

From an initial defect size a_o one must determine critical flaw size a_c for fast fracture as shown in Equation (3).

$$a_o \rightarrow a_c$$
$$K_I \rightarrow K_{IC} \tag{3}$$

where:
K_I = Applied tensile mode I stress intensity factor
K_{IC} = Plane strain fracture toughness of material

For LCF, determine how many cycles for a_o to grow to a_c. For HCF, one must prevent crack growth. Consequently for HCF, $K_I < K_{th}$, where:

K_I = Stress intensity factor ksi
K_{th} = Threshold stress intensity factor range below which fatigue crack growth (or corrosion fatigue crack growth) does not occur.

Further discussion of fracture mechanic concepts can be found elsewhere (Dowson, 1995, 1994).

Creep Rupture and Stress Rupture

Evidence of creep damage in the high temperature regions of blade attachment areas of rotors has been observed in some instances (Bush, 1982). The rim stresses and metal temperature at these locations are assessed against the creep rupture data for that particular material. Traditionally one has used a Larson Miller (LM) plot of the type shown in Figure 4 as referenced earlier in the paper under *Disks* section.

The degree of safety margin depends on the user and what lower bound design curve is applied. Since these curves are based upon the chemistry, variation in chemistry for a particular material can have an effect on the Larson Miller curve. Also, Larson Miller curves are generally based upon creep rupture tests done for 10^4 to 3×10^4 hours and very few data at 10^5 hours. Consequently, the data for longer hours is generally extrapolated. Since most of the creep rupture data is done with smooth bar specimens, the effect of notch ductility at long-term service has not been done. Short term notched bars tests may fail to predict the onset of notch sensitivity. Notch sensitively is not an inherent property but depends on the temperature, stress, stress state, and strain rate.

In assessing remaining life of components due to creep, such as blade attachments, crack initiation is used as the criterion. However, with the emergence of fracture mechanics and an increasing need to extend life of components, application of crack growth, techniques have become common in the past decade.

For crack initiation as the fracture criteria, history-based calculation methods are often used to estimate life.

Methods for Crack Initiation Due to Creep

For the analytical method, one must have accurate operating history of the components, which may consist of temperature, applied loads, changes in operation, such as shut downs or

variation in speed or pressure. A simplistic estimation of the creep life expended can be made by assessing the relaxed long-term bore stresses and rim-stresses against the standard rupture data using the life fraction rule. The life fraction rule (LFR) states that at failure Equation (4):

$$\sum t_i/t_{ri} = 1 \quad (4)$$

when t_i is the time spent at a given stress and temperature and t_{ri} is the rupture life for the same test conditions.

This rule was found to work well for small changes in stress and temperature. However, for stress variations, actual rupture lives were lower than the predicted values. Consequently, the LFR is generally valid for variable-temperature conditions as long as changing creep mechanisms and environmental interaction do not interfere with test results. However, the possible effect of material ductility on the applicability of the LFR needs to be investigated.

Nondestructive Techniques

Conventional nondestructive evaluation (NDE) techniques fail to detect incipient damage that can be a precursor to crack initiation and subsequent rapid failure. However, there are other NDE techniques that have been developed for estimating the life consumption. These include microstructural techniques and hardness based techniques.

Metallographic Examination

Metallographic techniques have been developed that can correlate changes in the microstructure and the onset of incipient creep damage, such as triple point cavitation at the grain boundaries. For this technique, measurements by replication technique are taken on crack sensitive areas that are subjected to the higher temperatures and stresses. These areas are generally indicated by experience and analysis of previous damages.

The creep damage measured by replication is classified into four damage stages:

- Isolated cavities (A)
- Oriented cavities (B)
- Macrocracks (linking of cavities) (C)
- Formation of macrocracks (D)

Figure 44 shows the location of the four stages on the creep strain/exposure time curve (Neubauer and Wadel, 1983).

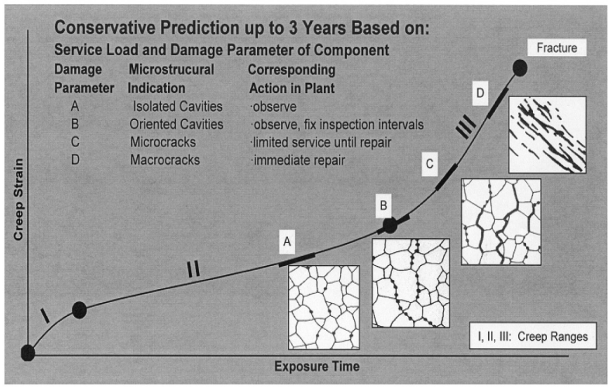

Figure 44. Replicas for Remaining Life Assessment.

In applying this approach Neubauer and Wadel (1983) classified the stages into five stages that are Undamaged, Stage A, Stage B, Stage C, and Stage D. These stages were corresponded roughly to expended life fracture ($t/_{tr}$) values of 0.27, 0.46, 0.65, 0.84 and 1, respectively, using the conservative lower bound curve. Consequently, the remaining life can be calculated using the relationship as shown in Equation (5):

$$t_{rem} = t(t_r/t - 1) \quad (5)$$

where:
t is the service life expended and t_r is the rupture life.

For undamaged material and damaged stages A, B, and C, the remaining life was found to be approximately 2.7t, 1.17t, 0.54t and 0.19t, respectively. Then by applying a safety factor of 3 to the calculations, the safe reinspection intervals will become 0.9t, 0.4t, 0.18t and 0.06t respectively. This approach has been developed and implemented in the power generation industry (Viswanathan and Gehl, 1991). It was found to give increased inspection intervals as compared to the Neubauer and Wadel (1983) approach, as shown in Table 13.

Table 13. Suggested Reinspection Intervals for a Plant with 30 Years of Prior Service.

	Inspection Interval (Years)	
Damage Classification	**Wedel-Neubauer**	**EPRI-APTECH**
Undamaged	5	27
A. Isolated Cavities	3	12
B. Oriented Cavities	1.5	5.4
C. Linked Cavities (Microcracks)	0.5	1.8
D. Macrocracks	Repair Immediately	Based on fracture mechanics

This approach has been applied by several utilities and realized significant savings in inspection costs. Other investigations indicate that there are wide variations in behavior due to differences in grain size, ductility and impurity control (Carlton, et al., 1967). For conservatism, the authors' company adapted the Neubauer and Wadel (1983) approach and classified the five stages as follows:

1. Undamaged material: Equipment can run and be reinspected at next shutdown.

2. Class A—Reinspection would be three to five years.

3. Class B—Reinspection would be one and one-half to three years.

4. Class C—Replacement or repair would be needed within six months.

5. Class D—Immediate repair would be required.

Creep/Fatigue Interaction

For components that operate at higher temperature where creep growth can occur, one must take into account of the creep crack growth at intervals during the fatigue life of the component. For a more in-depth discussion of creep/fatigue interaction see (Dowson, et al., 2005)

High Temperature Corrosion

Fluid catalytic cracking hot gas expanders operate in environments that can be both corrosive and erosive. Although it is well documented that the source of erosion comes from the regenerated catalyst that is carried with the hot flue gas from the FCC, its effect on high temperature corrosion has only begun to be understood by the authors' company. Papers published by the author outline the relationship of stress and temperature on the high temperature corrosion/fracture mechanics of Waspaloy in various catalyst environments (Dowson, et al., 1995; Dowson and Stinner, 2000).

The nature of the corrosion attack is primarily influenced by the type of crude oil stock, which in time has a bearing on the resulting flue gas composition, regenerated catalyst and the nature and quality of additions injected into the FCC process.

When evaluating remaining life assessment of hot gas expanders especially the rotating components, one must consider the effect of the environment such as high temperature corrosion. The authors' company has developed a fracture mechanics model which

incorporated both the effect of oxide wedge formation and the apparent reduction in fracture toughness of Waspaloy in contact with the catalyst residue. By utilizing this model one can predict whether fracture will occur under various environmental/operating conditions of the hot gas expander. The authors' company periodically tests catalysts from end-users' hot gas expanders to determine if oxide wedge can occur and what life span to reach the critical size for failure. Generally, if the catalyst is active, then high temperature corrosion will occur. Consequently, a blade will be removed from the unit and examined metallographically to determine the oxide wedge depth. Based upon the depth and time of operation, the remaining life can be estimated (Figure 45). This figure is also shown as Figure 27.

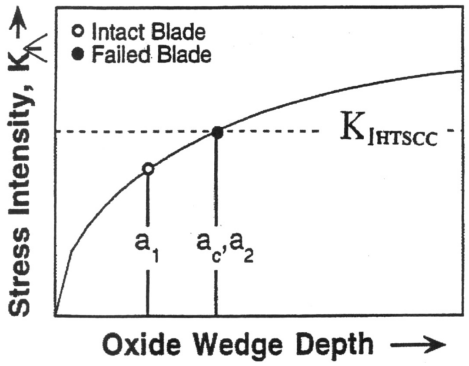

Figure 45. Stress Intensity Profile Versus Oxide Wedge Depth for Unit A. Critical Oxide Wedge Depth for Failure Was Defined as a_c. In the Failed Blade, a_2 Was Found to Exceed a_c. In an Intact Blade, a_1 Was Less Than a_c.

CASE STUDY 1—REMAINING LIFE ASSESSMENT OF HOT GAS EXPANDER DISK

A life assessment was performed on a disk from a large hot gas expander that had been in operation for approximately 51,000 hours of service. The present life assessment was necessary to ensure that the properties of the disk had not degraded with time. This life assessment consisted of a microstructurally evaluation as well as mechanical testing.

Replicas of the microstructure of the disk were taken from five locations shown in Figure 46 and subsequently examined via optical microscope. A blade root from the disk that had seen the same accumulation of time was also sectioned, metallographically prepared using the standard techniques, and examined. Specifically the microstructure was examined in the area of the first, third, and fourth landings. Also specimens were also prepared to examine corrosion products.

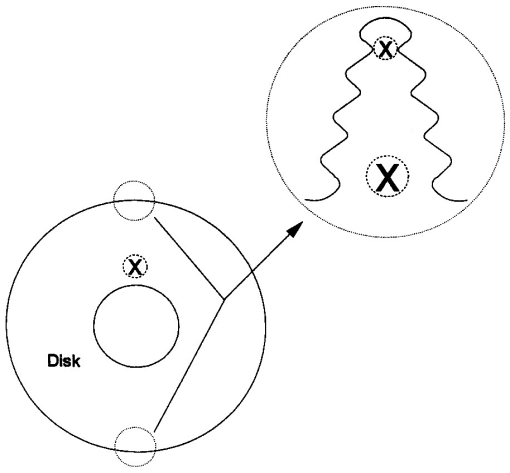

Figure 46. Diagram Indicating Location of Disk Replicas.

Representative micrographs of the microstructure of the root of the blade and of the disk may be seen in Figure 47. The structure was found to be uniform and typical for A286 with an ASTM grain size ranging from four to six. No creep voids were observed.

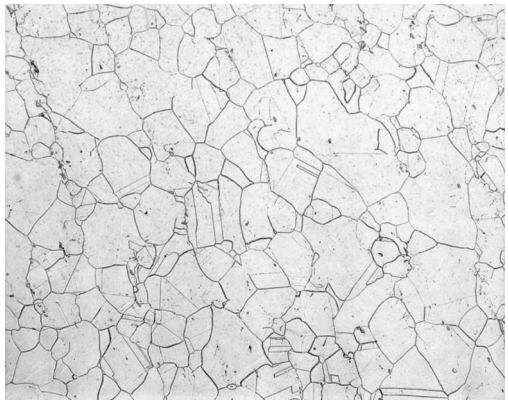

Figure 47. Optical Micrograph of Typical Microstructure of Root of Blade #38. (15 ml HCI, 10 ml HN03, 10 ml Acetic Acid, 100×).

Several areas of high temperature corrosion arrack were evident in the area of the first and third root lines of the blade that was sectioned. A micrograph of this corrosion may be seen in Figure 48.

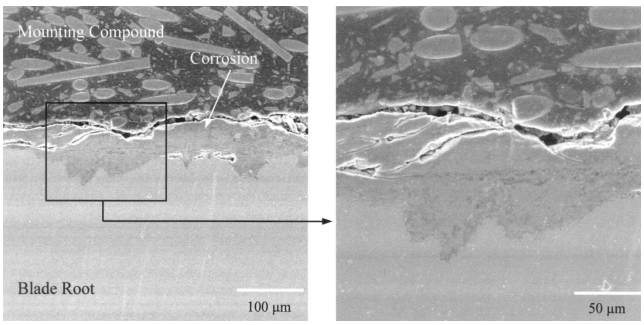

Figure 48. SEM Micrographs of Cross Section of Corrosion Seen in Radius of First Root Landing of Blade #38.

The maximum depth of penetration of corrosion product was found to be approximately 100 micrometers. No corrosion product was observed in areas removed from this accelerated attack, which suggests that a thin Cr_2O_3 layer had formed over the surface of the majority of the blade root and remained protective. This type of corrosive attack is expected for an iron chromium based alloy exposed to an atmosphere consisting of a mixture of sulfur and oxygen. Many high temperature alloys including A286 rely on the formation of the compact slow growing chrome oxide scale for protection from the environment. Exposure to sulfur may lead to the breakdown of this protective scale providing the necessary conditions of temperature and pressure exists. The nature of the corrosive products that form dependent on both thermodynamic and kinetic factors, the details of which are beyond the scope of this paper. A more detailed description of the mixed oxidants is given by Dowson, et al. (1995), and Birks and Meier (1983).

It is not uncommon to see corrosion in the areas of blade root described in Figure 49. One explanation of this is that in these areas there is a gap between the blade root and the disks that allows catalyst into the blade root area. The presence of this catalyst may lead to high temperature corrosion as described by Dowson, et al. (1995), and Dowson and Stinner (2000). Some corrosion was also seen on the context surface of the land that is being proposed that corrosion in these areas is exacerbated by fretting. However, in this investigation this type of corrosion occurred to a much lesser extent than seen in the areas mentioned previously.

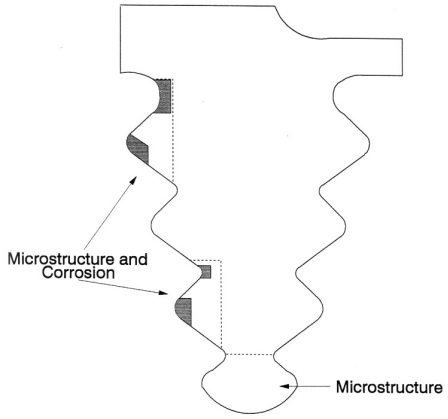

Figure 49. Diagram Indicating Sectioning of Blade Root and Location of Corrosion.

Because destructive testing could not be preformed on the actual disk material samples for stress rupture testing were taken from the root lower airfoil of the blade as shown in Figure 50. It was assumed that the properties of the sample are similar to those of the disk roots. Modified stress rupture tests as developed by Dowson, et al. (1995), and Dowson and Stinner (2000) were also performed in order to determine if the corrosion products seen in the blade root area would cause cracking of the disk.

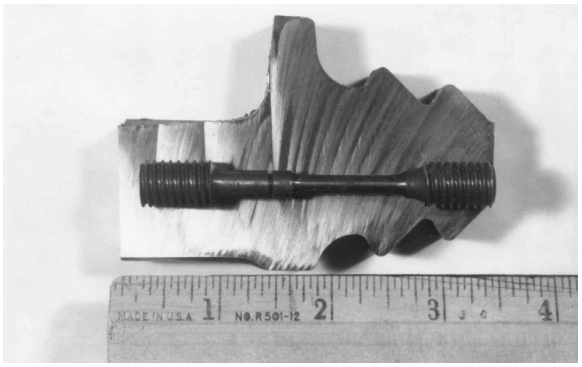

Figure 50. Photograph Illustrating Locating from Which Rupture Specimen Was Taken Relative to the Blade Root/Lower Airfoil.

The stress rupture specimen from the blade was found to have an elongation of 10 percent and a reduction of area of 14 percent. The fracture occurred in the smooth section of the bar after 195.5 hours. This meets the authors' company specification, which requires that the specimen last at least 30 hours with rupture occurring in the smooth section and possess an elongation of at least 10 percent. The mill certification of the original blade material gives an elongation and reduction in area of 11.7 and 19 percent, respectively, which is comparable to the present results. Thus the rupture properties of the disk have not been significantly degraded as a result of operation of the expander.

Modified Stress Rupture Testing

This test developed by Dowson, et al. (1995), is used to determine the stress to cause fracture of the disk material in the presence of spent catalyst. The stress may be converted to a stress intensity that may be compared to the stress intensity at the tip of the "wedge" created by the corrosive product. A determination may then be made as to whether cracking in the disk will occur. It was found that the presence of spent FCC catalyst may greater reduce the rupture strength of Waspaloy. For example, a sample test of 1200°F (649°C) and a stress of 95 ksi lasted over 900 hours when tested in air while the same temperature and stress produced failure in only three hours when the sample was tested in the presence of catalyst. In the present investigation, initial test of 1200°F (649°C) and a stress of 54 ksi confirmed that A286 is also susceptible to this type of degradation. The sample failed in only 4.25 hours as opposed to 500 hours as predicted by the authors' company material property database for stress rupture in air. Therefore, in order to get an accurate assessment of the rupture properties of the disk in the area of the root in question, the modified stress rupture test was used by Dowson and Stinner (2000). In the case at hand a temperature of 1065°F (574°C) was chosen for the test based on the temperature of the disk rim at the point of maximum stress, which was determined by finite element analysis to be in the radius of the fourth root landing. The stress used in the tests range from 62 to 102 ksi. Each test consists of an exposure of stress and temperature for at least 20 hours. If the specimen did not break it was unloaded and the catalyst replaced and then retested at a stress that was increased by 10 ksi. This process that was repeated until fracture occurred at a stress of 102 ksi, which corresponds to a stress intensity of 24.27 ksi$\sqrt{}$in. It should be noted that the catalyst that was used is kept at the authors' company for testing purposes, i.e., it was not from the actual end users unit. It is likely that this test catalyst was much more contaminated than the end users catalyst, which will result in lower values of rupture stress than if the actual end users catalyst was used.

In order to determine the stress intensity of the tip of the corrosion wedge it was first necessary to determine the stress profile. The σ (X) of the area of the root in question, the stress intensity may be calculated from Equation (6) as referenced earlier in the paper as Equation (1).

$$K_I = \int_0^a \sigma(x)m(x,a)dx \qquad (6)$$

where:
a is the wedge depth and the X is the coordinate dimension.

The term M (x, a) is the weight function, which is dependent on the geometry of the cracked body. When considering the corrosion, wedge formed within the area of a disk rim, the geometry may be approximated as an edge crack in a semi-infinite plate, shown in Equation (7), as referenced earlier in the paper as Equation (2):

$$m(x,a) = \frac{2}{\sqrt{2\pi(a-x)}}\left[1 + .5693\left(1-\frac{x}{a}\right) + .279375\left(1-\left(\frac{x}{a}\right)^2\right)\right] \qquad (7)$$

A linearized stress field of the fourth root landing of the disk rim of the end users expander was determined by a finite element analysis. From these data an expression of σ (X) was derived and the integral of Equation (6) evaluated to give the stress intensity at the tip of the corrosion wedge. The results of these calculations are summarized in Figure 51, which is a plot of stress intensity versus corrosion wedge depth.

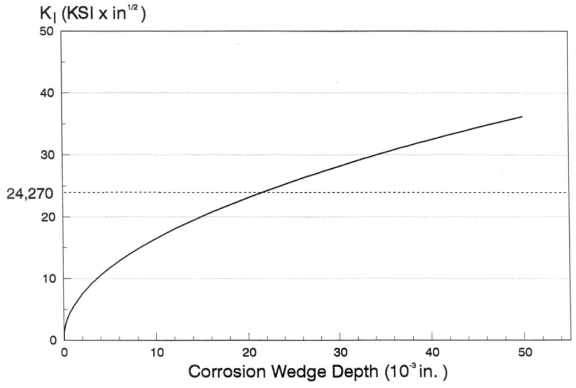

Figure 51. Stress Intensity Versus Corrosion Wedge Depth for Fourth Root Landing of Disk.

Based on this plot, a corrosion wedge will have to penetrate to an approximate depth of .021 inches before the critical stress intensity is exceeded and catastrophic fracture occurs. As mentioned, the maximum penetration seen was approximately .004 inches. Because the growth of the corrosion product is parabolic, e.g., the growth slows with time, it is unlikely that the corrosion would cause a failure of the disk providing the temperature and atmosphere of the expander are not changed significantly.

Conclusions

The microstructure in the ruptured product has not been significantly affected by the operation of the expanders. Some high temperature corrosion was seen in the root area, however, this has been determined that this corrosion will not result in the failure of the disk. Therefore, the disk will be used without significant risk of failure. It is recommended that this be reevaluated after an operational period of four to five years.

CASE STUDY 2—REMAINING LIFE ASSESSMENT OF THE POWER RECOVERY HOT GAS EXPANDER

Remaining life assessment testing was performed on a large expander disk, which had been in operation approximately 85,000 hours of service. This FCC hot gas expander first began operating in December 1995 and has been in continuous operation until 2005. Operational data provided by the customer reveal that this unit has run with a consistent inlet temperature of 1296.6°F (703°C). Only one significant afterburn was reported by the customer, which may have caused the temperature of the gas upstream of the expander to reach a temperature of 1467°F (797°C) for three days. This expander had not caused any outages since it was placed into service, however, there have been a few FCC outages.

During a September 2000 turnaround at the customer site, the authors' company performed a remaining life assessment test, which was based completely on fracture mechanics and a visual inspection of the disk and blades. The analysis concluded that an insignificant amount of the fatigue life of the blades had been used.

In preparation for a September 2005 turnaround, the authors' company was again contracted to perform a remaining life assessment study. This assessment included the testing of Waspaloy stress rupture samples in the presence of FCC unit catalyst in order to determine if the impurities trapped in the catalyst were hazardous to the expander disk and blades. The results of the catalyst testing were inconclusive, and it was recommended that a thorough investigation of the extent of the corrosion product on the blades be preformed.

Remaining life assessment testing was performed on the expander disk at the authors' company service facility. This included examination of the microstructure of the disk roots by taking replicas as well as hardness readings. Two of the blades were removed from the disk and were cut so that stress-rupture, stress relaxation testing, and constant displacement rate testing samples could be obtained. One of these blades was re-solution treated and aged so that the results could be compared against samples cut from the blade in the as-serviced condition. The blades removed from the disk were the original blades supplied with the unit, so they have seen the same service life and service conditions as the disk.

Metallurgical Examination and Discussion

Metallurgical Examination of the Disk

Pictures of the inlet and exhaust faces of the disk are given in Figures 52 and 53. During the metallurgical evaluation, the microstructures on both the inlet and the exhaust faces of the disk were examined. An illustration of the points where the microstructures were inspected is given in Figure 54. There were 10 areas examined on both the inlet and exhaust face, making a total of 20 examined locations. These areas were polished and etched to reveal the microstructure of the material. Using a rubberlike resin substance, replicas of the microstructures were taken from each of these 20 locations that were then examined using an optical stereoscope.

Figure 52. Picture on the Inlet Face of the Expander Disk.

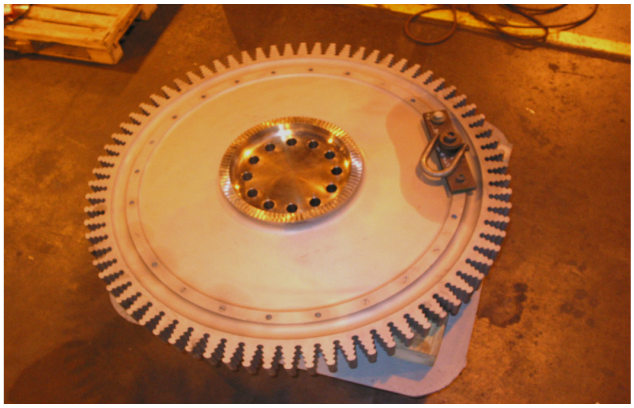

Figure 53. Picture of the Exhaust Face of the Disk.

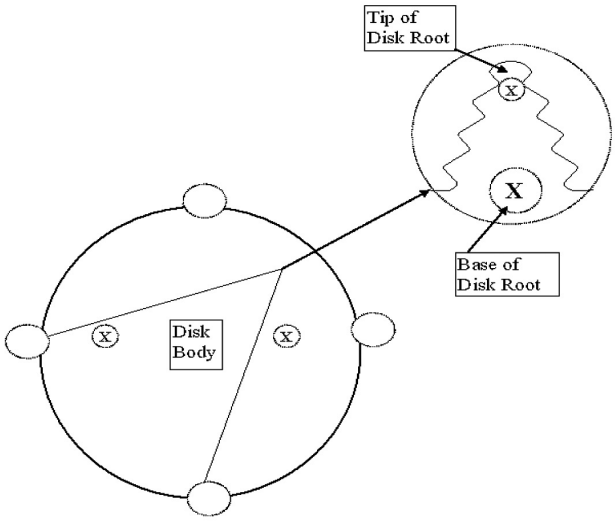

Figure 54. Diagram Illustrating the Locations of the Disk from Which Replicas Were Taken. All 10 Areas Were Examined on Both the Inlet and Exhaust Faces of the Disk.

Photomicrographs of the microstructures obtained from the replicas are shown in Figures 55 through 60. The microstructure of the disk is consistent at all locations on both the inlet and exhaust faces of the disk. The average grain size at all locations on the disk is ASTM 5.5, which meets the requirements of the authors' material specification. The consistency of the microstructure is a

good indication that the disk was not exposed to excessive heat during service. The microstructure displays no evidence of creep damage as there are no voids at the grain boundary triple points.

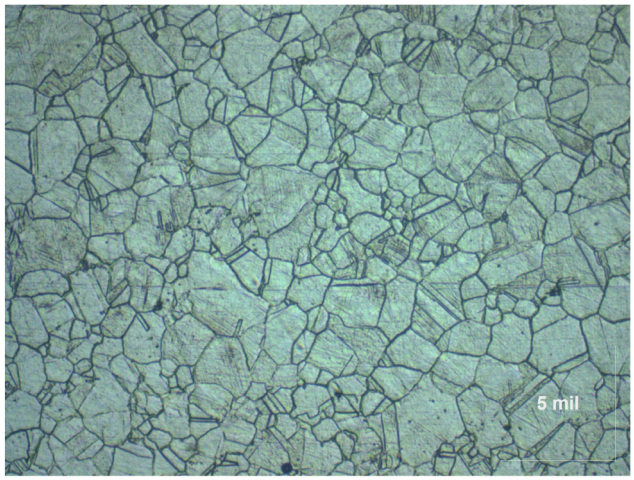

Figure 55. Inlet Face—Tip of Disk Root. Photomicrograph Taken from Replica.

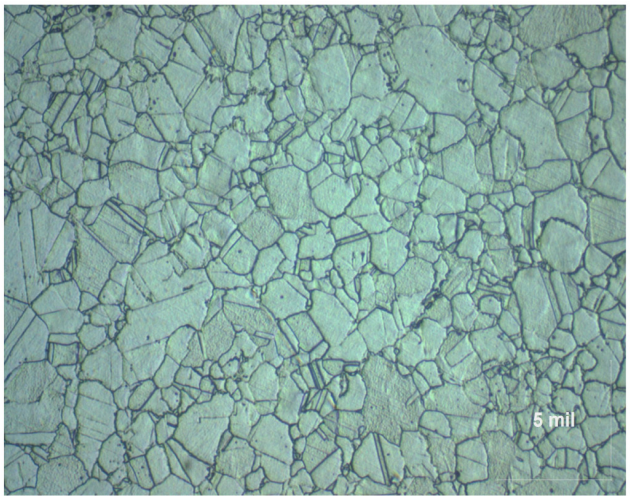

Figure 56. Inlet Face—Base of Disk Root. Photomicrograph Taken from Replica.

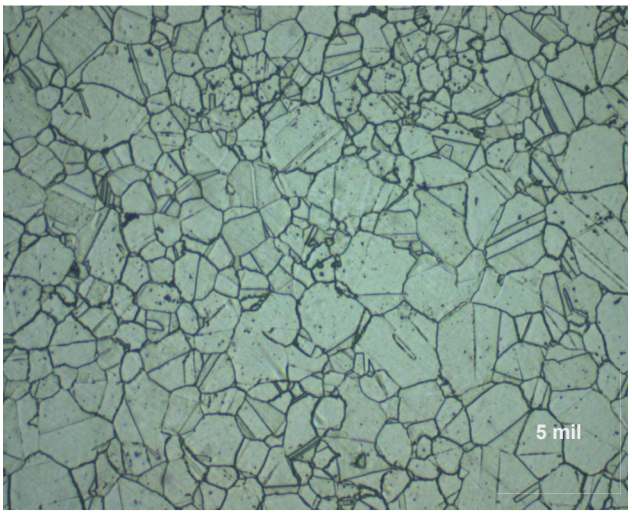

Figure 57. Inlet Face—Disk Body. Photomicrograph Taken from Replica.

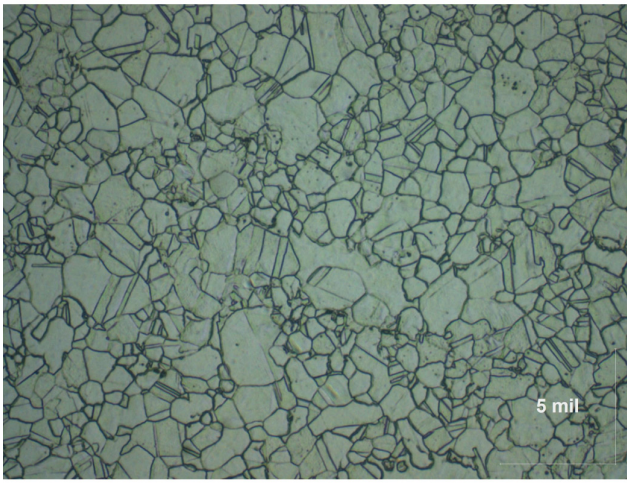

Figure 58. Exhaust Face—Tip of Disk Root. Photomicrograph Taken from Replica.

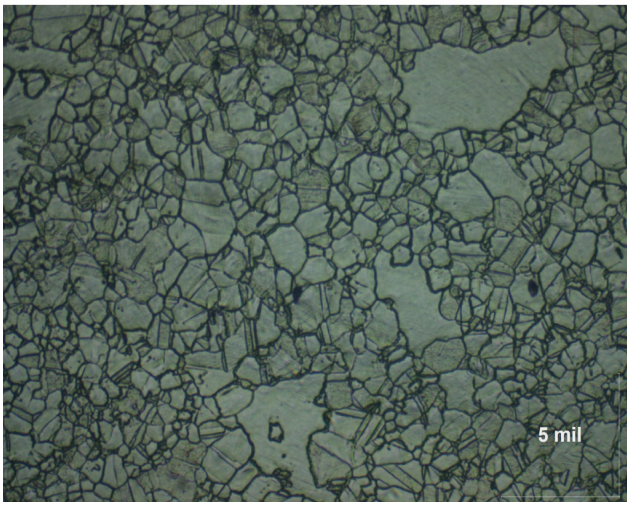

Figure 59. Exhaust Face—Base of Disk Root. Photomicrograph Taken from Replica.

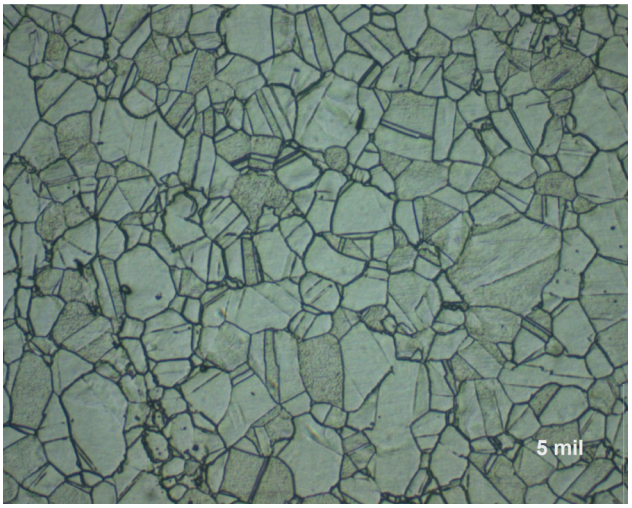

Figure 60. Exhaust Face—Disk Body. Photomicrograph Taken from Replica.

Hardness readings were taken on all of the examined areas of the disk using a hardness tester. The average hardness readings taken at each location are shown in Table 14. The hardness readings are

consistent at all locations on both faces of the disk, and all meet the requirements of the authors' material specification. This provides further evidence that the disk was not exposed to excessive heat during operation.

Table 14. Average Hardness Values at Examined Disk Locations.

	Inlet Face	Exhaust Face
Tip of Disk Root	37.7 HRC	38.2 HRC
Base of Disk Root	39.4 HRC	40.9 HRC
Disk Body	39.8 HRC	40.1 HRC
Note: Hardness readings were taken with Equo-Tip III Hardness tester and converted to HRC hardness values.		

Metallurgical Examination of the Blades

Two of the blades were taken out of service for destructive testing. One of the blades was re-solution treated and aged according to the authors' material specification for examination and destructive testing, while the other blade was tested in the condition it was in as it was pulled from service. In this report, the service blade that was not reheat treated will be referred to as the "service condition" blade while the blade that was re-solution treated and aged will be referred to as the "reheat treated" blade. The blades are also made from the authors' material specification and the blade roots are exposed to higher stresses during service than the disk roots, making examination of the blades a conservative representation of the current conditions of the disk while allowing for destructive testing.

Sections from the root of the service condition blade and the reheat treated blade were cut and polished for examination under an optical microscope. Photomicrographs of the microstructures of these blade roots are shown in Figures 61 and 62. The photomicrographs show that the average grain size of both blade roots is ASTM 4, which is slightly larger than the average grain size of the disk, however, this grain size still meets the requirements of the authors' material specification. Again, no evidence of creep damage or exposure to temperatures beyond the designed service temperature could be found. There is a slight difference between the grain boundaries of the as-serviced blade and the reheat treated blade under higher magnification. The grain boundaries of the service condition blade, shown in the photomicrograph in Figure 63, reveal that the grain boundaries contain continuous films of carbides. This is evidence that carbides are precipitating at the grain boundaries. These observations are illustrated by comparison to the microstructure of the reheat treated blade, which is shown in the photomicrograph in Figure 64. The grain boundaries of the reheat treated blade are more discrete and there are fewer precipitates present at the grain boundary locations.

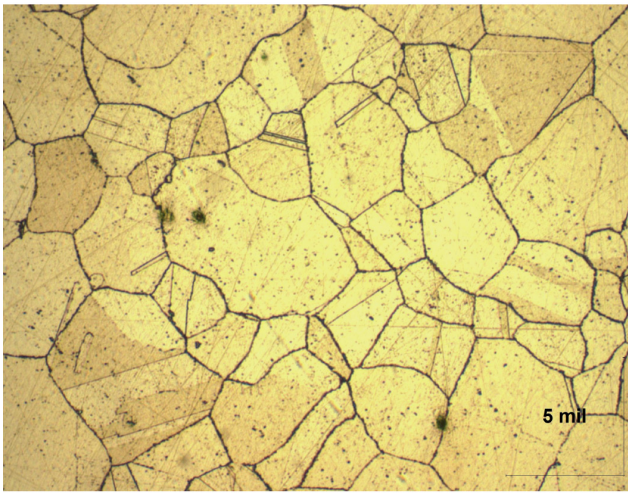

Figure 61. Photomicrograph of Service Condition Blade Root.

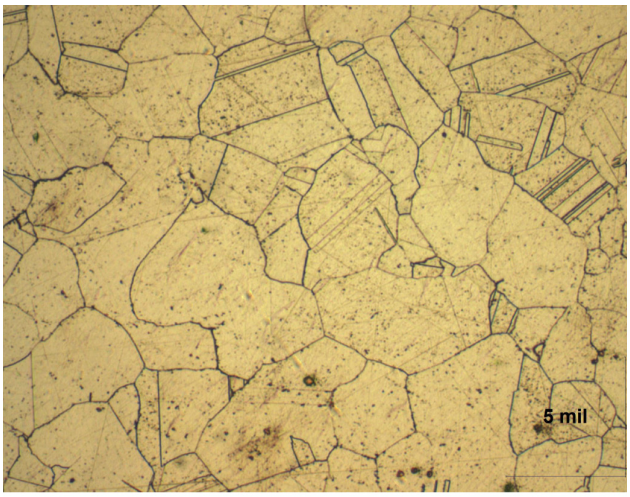

Figure 62. Photomicrograph of Reheat Treated Blade Root.

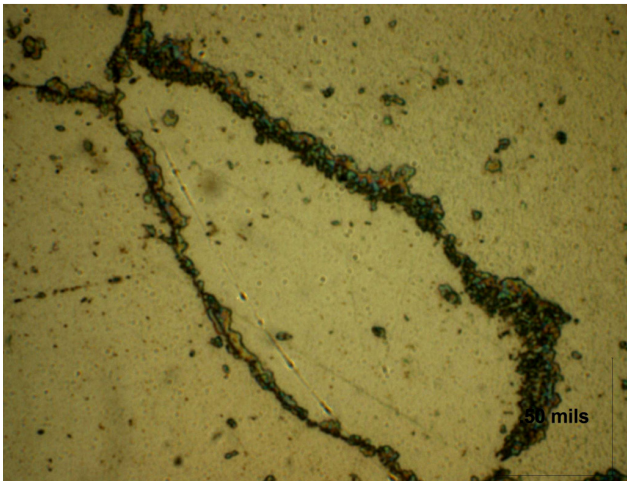

Figure 63. Photomicrograph of Grain Boundary on Service Condition Blade Root.

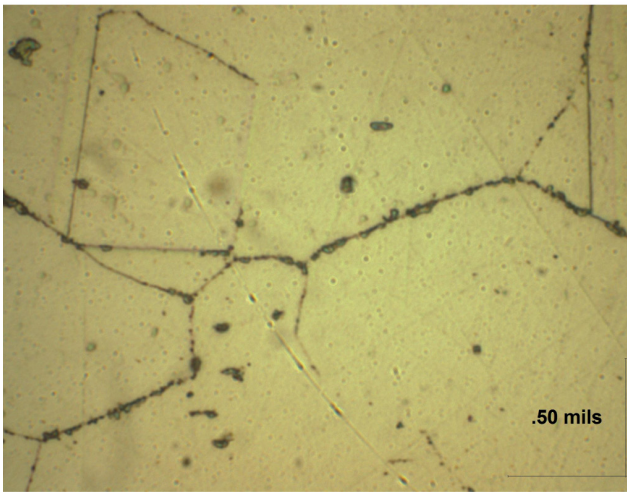

Figure 64. Photomicrograph of Grain Boundary on Reheat Treated Blade Root.

Corrosion Testing

In order to accurately measure the depth of the corrosion product at the blade root, cross-sectional samples along the top inside radius were cut according to Figure 65. The five samples were mounted and polished for examination under an optical microscope.

Corrosion wedges, as seen in Figure 66, were found along this inside radius. The deepest corrosion wedge located at the center along this inside radius is shown in Figure 66, and depth of the corrosion wedge is 0.0043 inches (4.3 mils).

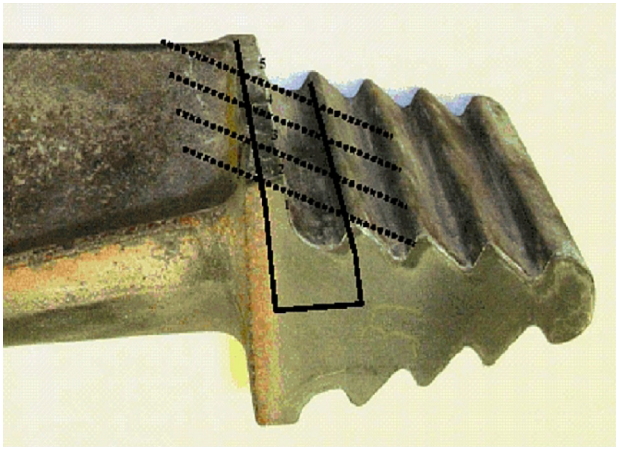

Figure 65. Location of Cross-Sectional Samples Cut to Examine Corrosion Wedge.

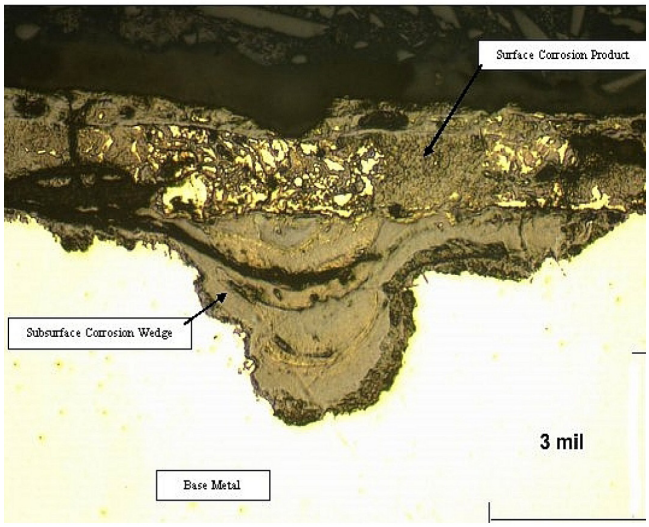

Figure 66. Photomicrograph of Deepest Corrosion Wedge Found in the Blade Root. Depth of Corrosion Wedge = 4.3 mils.

Using a scanning electron microscope (SEM), energy dispersive spectroscopy (EDS) was performed on the corrosion product. The results of the EDS analysis, shown in Figures 67 and 68 indicate that the corrosion product on the surface of the Waspaloy is NiO and NI_3S_2 while the subsurface corrosion product is Cr_2O_3 and Cr_2S_3.

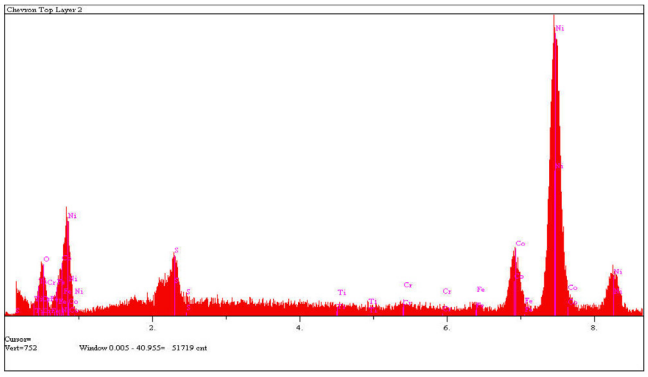

Figure 67. EDS Scan Taken on Top Corrosion Layer in Figure 66.

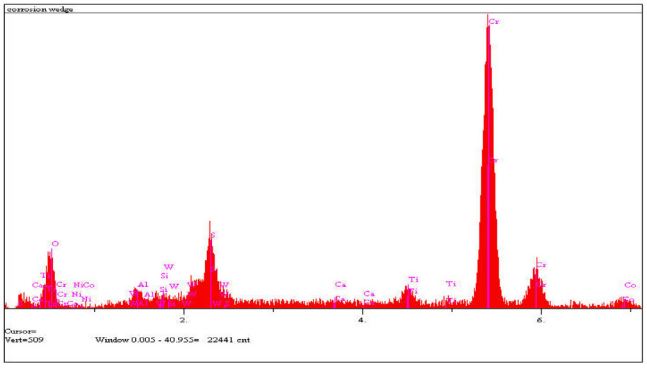

Figure 68. EDS Scan Taken on Subsurface Corrosion Wedge in Figure 66.

The evidence of these corrosive products indicates that high temperature corrosion is occurring but at a slow rate. By applying the parabolic rate, Equation (8), one can determine the growth of the oxide wedge with time.

$$X2 = [\ kp * t\ ] / 2 \qquad (8)$$

Based on the applied stress at the blade root a plot of stress intensity K_I verses oxide wedge depth is plotted. Since the unit is operating in a fully combustion state and that the spent catalyst was not contaminated, a critical stress intensity K_{IC} of 16 ksi$\sqrt{in}$ was applied to the curve (Figure 69). From this curve K_I will reach K_{IC} when the oxide wedge is 0.015 inch depth. Also the time for this depth of growth would take over 10,000 years. This calculation assumes that all service parameters such as operating temperature and gas/catalyst analysis remains unchanged.

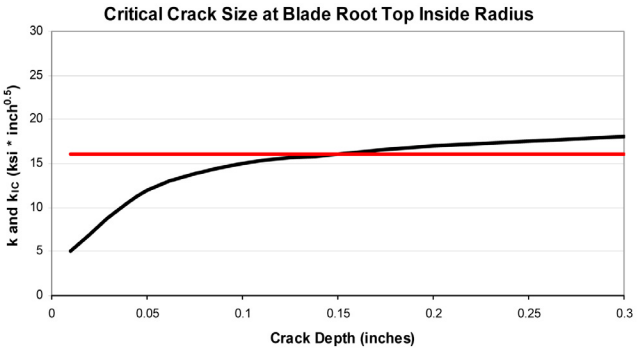

*Figure 69. Stress Intensity Factor Versus Crack Depth at the Top Neck of the Blade Root. The Critical Crack Depth Corresponding to k_{IC} = 16 ksi*inch$^{0.5}$ is 0.15 inches.*

Stress Rupture Testing

Stress rupture testing was performed on a sample cut from the service condition blade root as well as the reheat treated blade root. The stress rupture bars where standard smooth/notch combination bars and were machined in accordance to ASTM E292 Specimen #4. The results of the stress rupture testing are given in Table 15.

Table 15. Stress Rupture Results of Inservice and Reheat Treated Blade.

Stress Rupture Testing 1350°F (732°C) at 75,000 psi stress			
	Time to Fracture	% Elongation	Fracture Location
Service Condition Blade	40.44 hours	23%	Smooth
Reheat Treated Blade	70.34 hours	9%	Smooth

Both samples fractured in the smooth section of the bar indicating that the material has adequate notch ductility. Although the reheat treated sample had a longer time to rupture, the ductility of the material had dropped in comparison to the as-serviced blade.

Stress Relaxation Testing and
Constant Displacement Rate Testing

The stress relaxation testing (SRT) and constant displacement rate testing (CDR) were performed on the as-received blade and a blade that was re-solution treated and aged. The blades removed from the disk were the original installed blades, which had seen 85,000 hrs. The SRT tests were done over a temperature range of 1112°F to 1472°F (600°C to 800°C) at 0.4 percent and 1.3 percent total strain. The stress relaxation tests on Waspaloy from serviced blades and also after reheat treatment were analyzed in terms of stress versus creep rate and compared directly with previous data for standard Waspaloy. For the two conditions, the creep strength showed a crossover depending on the test temperature or creep rate (or time). However for both conditions in the current test comparison with the standard Waspaloy was favorable. This suggests no significant loss in creep strength resulted from the service exposure (Figure 70 and Figure 71).

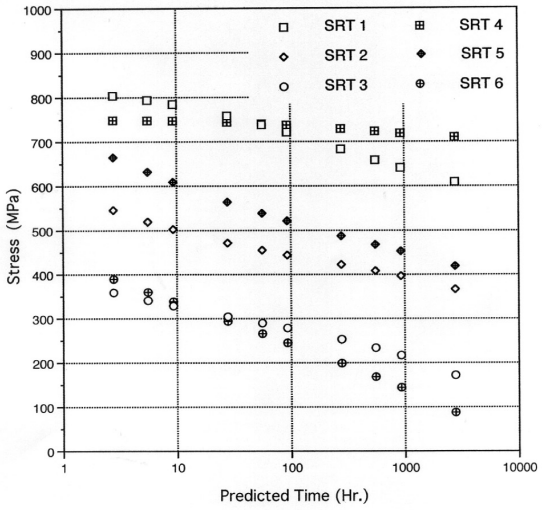

Figure 70. Stress Versus Predicted Time for 1 Percent Creep Comparison Between Service Condition Blade and Reheat Treated Blade.

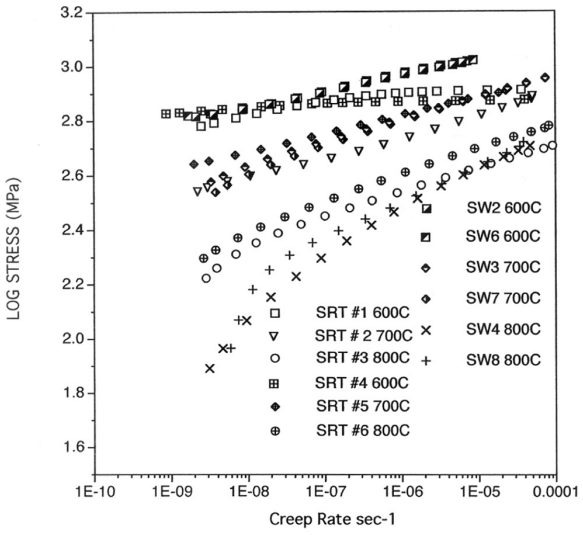

Figure 71. Log Stress Versus Creep Rate Curves Comparing the Service Condition Blade and the Reheat Treated Blade with Standard Waspaloy Samples.

The CDR tests were conducted at 1112°F and 1202°F (600°C and 650°C) where ductility is expected to be near a minimum and where the alloy is most vulnerable to fracture. The results are shown in Figure 72. From the curve the reheat treated condition has a higher notch displacement at fracture and at 1202°F (650°C) a greater amount of unloading. Although a certain amount of embrittlement has occurred with the service exposed Waspaloy, the remaining material still has adequate notch ductility as shown by stress rupture test for the service condition blade as compared to the reheat treated blade. The authors' company conclusion from the remaining life assessment testing is that the disk is suitable for future service under the current operational conditions of the unit. The authors' company recommends that this disk receive another remaining life assessment after five to six years of operation.

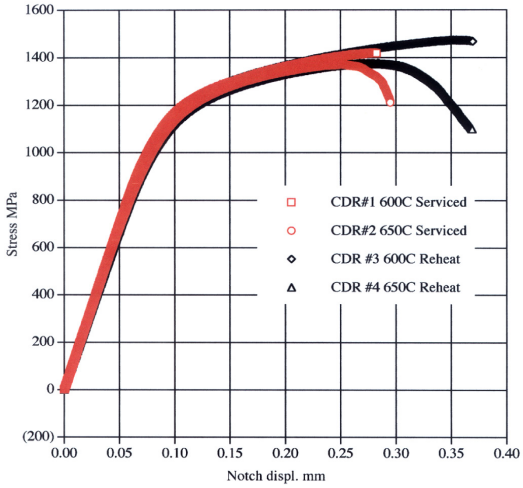

Figure 72. CDR Results at 1112°F and 1202°F (600°C and 650°C) for Service Condition Blade and Reheat Treated Blade.

SUMMARY

A review of materials and materials related processes has been presented for hot gas expander components. Special attention has been given to address some of the material issues like high temperature corrosion and/or embrittlement that can occur in operating at these high temperatures. Also highlighted are steps that one can take to prevent and/or minimize reoccurrence of these issues.

By applying remaining life assessment techniques and fracture mechanics concepts, one can evaluate in service units and assess their capabilities for further operation.

What will the future bring for new materials or new techniques for manufacturing high temperature components? The application of refined existing processes such as powder metals (P/M) net shape, hot isostatic pressing (HIP) process or laser microwelding of metallic powders to blade tips.

APPENDIX A

The following procedures are prepared for a unit or equipment that is being shut down for a normal turnaround inspection and repair. It assumes the equipment will be opened and exposed to the atmosphere. Protection of the equipment is provided by washing with a sodium carbonate solution before exposure to the atmosphere. The carbonate film must be maintained on the equipment during the downtime period.

1. Follow normal procedure to free the unit of hydrocarbons.
2. Before the temperature of gas/steam in the unit reaches the condensing temperature, add NH_3 to the steam at a rate to give 5000 wppm.
3. Circulate a sodium carbonate (soda ash) solution through the equipment for two hours minimum.

a. Solution to contain 2 wt percent Na_2CO3, 0.5 wt percent sodium nitrate and 0.05 wt percent wetting agent.

b. Maintain concentration of Na_2CO3 at 2 wt percent in the circulating solution as it will be depleted neutralizing the polythionic acid. This is particularly important when there are packed towers or catalyst beds.

c. During circulation, check vents and drains to assure all surfaces are being contacted by the carbonate solution.

4. Drain the carbonate solution and open the equipment for inspection or repair.

a. Carbonate solution must dry on the equipment to provide continued protection against accidental moisture contact.

b. Any equipment not to be inspected should remain closed to protect the surface.

c. After inspection or repair, equipment should be closed.

d. Equipment must not be washed with water. If washing or flushing is required, the sodium carbonate solution must be used.

5. The gas/steam used for startup must have 5000 wppm NH_3 added while condensation can occur in the equipment or until the unit is free of oxygen (a dry inert gas purge can be used).

REFERENCES

ASME Boiler & Pressure Vessel Code - Section II, 2007, Materials, Part D Properties, American Society of Mechanical Engineers, New York, New York.

ASTM A240, 2008, Table 1, American Society for Testing and Materials, West Conshohocken, Pennsylvania.

ASTM Task Group Report on A286, 1981/1982, American Society for Testing and Materials, West Conshohocken, Pennsylvania.

Birks, N. and Meier, G. H., 1983, *Introduction to High Temperature Oxidation of Metals*, London, England: Edward Arnold Publishers.

Bush, S. H., 1982, *Failures in Large Steam Turbine Rotors, in Rotor Forgings for Turbines and Generators*, R. I. Jaffe, Editor, New York, New York: Pergamon Press, pp. I-1 to I-27.

Carlton, R. G., Gooch, D. J., and Hawkes, B. M., 1967, The Central Electrical Generating Board Approach to "The Determination of Remanent Life of High Temperature Turbine Rotors," I. Mech E. Paper C300/87.

Darmara, F. N., December 1967, *J Metals*, pp. 42-48.

Dowson, P., 1994, "Fitness for Service of Rotating Turbomachinery Equipment," 10th Annual North American Welding Research Conference, Columbus, Ohio, October 3-5.

Dowson, P., 1995, "Fracture Mechanics Methodology Applied to Rotating Components of Steam Turbines and Centrifugal Compressors," Third International Charles Parson Turbine Conference, Materials Engineering in Turbine and Compressors, 2, pp. 363-375.

Dowson, P. and Stinner, C., 2000, "The Relationship of Stress and Temperature on High-Temperature Corrosion Fracture Mechanics of Waspaloy in Various Catalyst Environments," *Proceedings of High Temperature Corrosion and Protection*, Materials at High Temperatures, 18, (2), pp. 107-118.

Dowson, P., Rishel, D. M., and Bornstein, N. S., 1995, "Factors and Preventive Measures Relative to the High Temperature Corrosion of Blade/Disk Components in FCC Power Recovery Turbines," *Proceedings of the Twenty-Fourth Turbomachinery Symposium*, Turbomachinery Laboratory, Texas A&M University, College Station, Texas, pp. 11-26.

Dowson, P., Wang, W., and Alija, A., 2005, "Remaining Life Assessment of Steam Turbine and Hot Gas Expander Components," *Proceedings of the Thirty-Fourth Turbomachinery Symposium*, Turbomachinery Laboratory, Texas A&M University, College Station, Texas, pp. 77-92.

Glinka, G. and Shen, G., 1991, "Universal Features of Weight Functions for Cracks in Mode I," *Engineering Fracture Mechanics*, *40*, (6), pp. 1135-1146.

Izenson, M. G., Swift, W. L., and Aungier, R. H., June 1994, "Sealing Flow Requirements for a Rotating Disk with External Swirling Flow," Presentation at the International Gas Turbine and Aeroengine Congress and Exposition, The Hague, Netherlands, pp. 1-12.

Kofstad, P., 1988, *High Temperature Corrosion*, New York, New York: Elsevier Applied Science, pp. 465-510.

Kolts, J., 1987, "Environmental Embrittlement of Nickel-Base Alloys," *Metals Handbook 9th Edition*, ASM International, Metals Park, Ohio, pp. 647-652.

Neubauer, E. and Wadel, V., 1983, "Rest Life Estimation of Creep Components by Means of Replicas," *Advances in Life Prediction Methods*, D. A. Woodford and J. E. Whitehead, Editors, New York, New York: ASME, pp. 307-314.

Nieskens, M., Khouw, F., Borley, M., and Roebschlaeger, K-H. W., June 1990, "Shell's Resid FCC Technology Reflects Evolutionary Development," *Oil & Gas Journal*, *37*, pp. 37-44.

Samians, C. H. and Kinoshita, K., et al., 1975, "Sensitization and Stabilization of Type 321 Stainless Steels Corrosion/75," (4).

Sehitoglu, H., 1992, "Thermo-Mechanical Fatigue Life Prediction Methods," *Advances in Fatigue Lifetime Predictive Techniques*, ASTM STP 1122, M. R. Mitchell and R. W. Landgraf, Editors, American Society for Testing and Materials, Philadelphia, Pennsylvania, pp. 47-76.

Shen, G. and Glinka, G., 1991, "Weight Functions for a Surface Semi-Elliptical Crack in a Finite Thickness Plate," *Theoretical and Applied Fracture Mechanics*, *15*, pp. 247-255.

Sih, G. C., 1965, "Cylindrical Bar with Circumferential Crack-Notch," *Handbook of Stress-Intensity Factors*, Bueckner, ASTM-STP 410 (1969).

Simms, C. T. and Hagael, W. C., 1972, *Superalloys*, JohnWiley & Sons, Ltd., pp.-66-67.

Sturley, R. A., Keller, H. F., and Cameron, J. A., 1981, *The Ranking of Power Recovery Turbine Blade Materials and Coatings for Resistance to Erosion*, New York, New York: The American Society of Mechanical Engineers.

Truman, J. R. and Kirby, W. H., et. al., 1960, "Some Ductility Aspects of 18-121Nb Steel," *Journal of the Iron and Steel Institute*, *196*, pp.-180-187.

Viswanathan, R. and Gehl, S. M., 1991, "A Method for Estimation of the Fracture Toughness of CrMoV Rotor Steels Based on Composition," ASME Transaction, *Journal of Engineering Mat. and Tech.*, *113*, April, pp. 263.

Xu, H., Hocking, M. G., and Sidky, P.S., 1993, "Sulphidation-Oxidation Behavior of a Ni-Co-Cr-Si Alloy in an SO_2 + O_2 Atmosphere," *Oxidation of Metals*, *39*, (5/6), pp. 371-388.

Xu, H., Hocking, M. G., and Sidky, P.S., 1994, "Sulphidation-Oxidation Behavior of Alloy 800H in SO_2-O_2 and H_2-H_2S-CO-CO_2 Atmospheres," *Oxidation of Metals*, *41*, (1/2), pp. 81-101.

Xu, W. and Carlsson, A. J., 1991, *Weight Functions and Stress Intensity Factor Solutions*, New York, New York: Pergammon Press.

Yakuwa, H., Narita, T., Kawasaki, M., Miyasaka, M., Fang, C., Go, T., and Nakahama, S., 1998, "Development of a Sulphidation-Corrosion Resistant Ni-Base Superalloy for FCC Power Recovery Turbine Rotors," *Proceedings of the Twenty-Seventh Turbomachinery Symposium*, Turbomachinery Laboratory, Texas A&M University, College Station, Texas, pp. 49-54.

ACKNOWLEDGEMENT

The authors are grateful for the support from the Materials Engineering Department and Global Technical Services and recognize Elliott Company for permission to publish the paper.